INFORMATION TO USERS

This manuscript has been reproduced from the microfilm master. UMI films the text directly from the original or copy submitted. Thus, some thesis and dissertation copies are in typewriter face, while others may be from any type of computer printer.

The quality of this reproduction is dependent upon the quality of the copy submitted. Broken or indistinct print, colored or poor quality illustrations and photographs, print bleedthrough, substandard margins, and improper alignment can adversely affect reproduction.

In the unlikely event that the author did not send UMI a complete manuscript and there are missing pages, these will be noted. Also, if unauthorized copyright material had to be removed, a note will indicate the deletion.

Oversize materials (e.g., maps, drawings, charts) are reproduced by sectioning the original, beginning at the upper left-hand corner and continuing from left to right in equal sections with small overlaps.

Photographs included in the original manuscript have been reproduced xerographically in this copy. Higher quality 6" x 9" black and white photographic prints are available for any photographs or illustrations appearing in this copy for an additional charge. Contact UMI directly to order.

ProQuest Information and Learning
300 North Zeeb Road, Ann Arbor, MI 48106-1346 USA
800-521-0600

UMI®

Université d'Ottawa · University of Ottawa

REGIONAL DEPOSITION AND DIAGENESIS OF LOWER ORDOVICIAN EPEIRIC, PLATFORM CARBONATES: THE ROMAINE FORMATION, MINGAN ARCHIPELAGO AND SUBSURFACE ANTICOSTI ISLAND, EASTERN QUEBEC

by

Patricia Brennan-Alpert

A thesis submitted to the Faculty of Science
In partial fulfillment of the requirements
For the degree of
Master of Science

Department of Earth Sciences
University of Ottawa
September 2001

© Patricia Brennan-Alpert, Ottawa, Canada, 2001

National Library of Canada
Acquisitions and Bibliographic Services
395 Wellington Street
Ottawa ON K1A 0N4
Canada

Bibliothèque nationale du Canada
Acquisitions et services bibliographiques
395, rue Wellington
Ottawa ON K1A 0N4
Canada

Your file Votre référence

Our file Notre référence

0-612-66016-8

The author has granted a non-exclusive licence allowing the National Library of Canada to reproduce, loan, distribute or sell copies of this thesis in microform, paper or electronic formats.

The author retains ownership of the copyright in this thesis. Neither the thesis nor substantial extracts from it may be printed or otherwise reproduced without the author's permission.

L'auteur a accordé une licence non exclusive permettant à la Bibliothèque nationale du Canada de reproduire, prêter, distribuer ou vendre des copies de cette thèse sous la forme de microfiche/film, de reproduction sur papier ou sur format électronique.

L'auteur conserve la propriété du droit d'auteur qui protège cette thèse. Ni la thèse ni des extraits substantiels de celle-ci ne doivent être imprimés ou autrement reproduits sans son autorisation.

Canada

Abstract

This study integrates Mingan Islands outcrop and Anticosti subcrop facies analysis with petrography and stable isotope geochemistry to establish a current framework for the Lower Ordovician Romaine Formation in the western Anticosti Basin. Inner to midshelf strata form a wedge, thinning from midshelf to inner shelf and from west to east. A basal transgressive unit onlaps Precambrian basement; it is overlain by muddy, bioclastic limestones and dolostones arranged in two depositional sequences. In the lower sequence the transgressive lag is overlain by a peritidal unit (not developed in the inner shelf), followed by a subtidal unit and a second peritidal unit; the sequence boundary is non-erosive. In the upper sequence, peritidal facies are overlain in the west by a second subtidal unit, which is truncated from west to east by the regional unconformity. In the inner shelf, carbonates are pervasively dolomitized; in the midshelf, peritidal units are pervasively dolomitized but subtidal units are partially dolomitized.

Petrography shows two stages of dolomitization, an early, synsedimentary to shallow burial stage characterized by planar replacement dolomites and a late stage characterized by nonplanar replacement dolomite, and pore and fracture filling dolomite cements. Stable Isotope data suggest two phases of late stage dolomitization, the first resulting from intraformational waters warmed by burial, and the second from warm basin derived brines.

Resumé

La Formation de Romaine (Ordovicien Inférieur) dans la partie ouest du Bassin d'Anticosti comprend une unité transgressive de base au-dessus du socle précambrien recouverte par des carbonates bioclastiques de milieu subtidal à peritidal et se distingue par deux séquences de déposition. La séquence supérieure est surmontée par une discordance régionale. Les strates représentant la plate-forme interne sont exposées dans l'Archipel de Mingan et caractérisées par faciès carbonatés complètement dolomitisés. Les strates représentant la plate-forme médiane et présentes en sous-surface de l'Île d'Anticosti montrent des faciès carbonatés de milieu péritidal complètement dolomitisés tandis que ceux de milieu subtidal sont partiellement dolomitsés.

Deux phases de dolomitisation se retrouvent régionalement incluant: i) un phase précoce synsédimentaire à enfouissement de faible profondeur caractérisée par des dolomies de remplacement à limite cristalline planaire et ii) une phase tardive caractérisée par des dolomies à limite cristalline non-planaire de remplacement et de cimentation de remplissage dans les fractures et les pores. La distribution et les caractéristiques pétrographiques et géochimiques des dolomies dans la région d'étude suggèrent que la première phase de dolomitisation s'est produite dans un milieu marin ou sous l'influence de fluides dérivés d'eau marine. Les dolomies tardives se sont probablement formées lors de l'enfouissement lorsque les fluides étaient de saumures dérivées du bassin.

Acknowledgments

This project was supported by the NATMAP project, Geological Bridges of eastern Canada, and by an Ontario Government Science and Technology Scholarship.

First thanks go to my supervisor, André Desrochers. Since he embodies the catalogue of virtues in a supervisor, I will only short-list a few favourite qualities here: generosity, diplomacy, great timing, and, best of all, that air of rational and good-humoured calm with which he approaches all problems.

Thanks to Denis Lavoie, my co-supervisor, for his energetic leadership in the workshops and field trips of the NATMAP-Geological Bridges of eastern Canada project and for his comments and suggestions on presentations and this manuscript. I am grateful to Guoxiang Chi at the Centre Géoscientifique Québec for sharing his expertise with me. A special thanks to Claude Morin, Géologue Pétroliér, at MRN Québec for making the cores, SOQIP and INRS materials available to me, for his enthusiasm and for being that friendly face at all the conferences. I am grateful to Esther Asselin for sharing her home, her magical city, la Ville de Québec, her friendship and her love of two languages.

At University of Ottawa, thanks to George Mrazek in the thin section lab, Wendy Abdi and Gilles St-Jean of the G. G. Hatch Isotope lab for their material assistance in this project. To Hélène De Gouffe many thanks for her help with all the administrative details.

And, last, thanks to Audrey Dallimore and Barbara Medioli for inspiration, organization, information and almost unfailing e-mail communication.

Table of Contents

List of Figures

List of Tables

INTRODUCTION

The Romaine Formation was deposited during the second and highest Cambro-Ordovician eustatic sea level rise, on the passive margin of the, then, equatorial and arid Laurentian continent (James *et al.*, 1982). The Romaine Formation is similar to other rock units of "the Great American Bank", as the Lower Ordovician carbonate platform has been called (Ginsburg, 1974, as cited in Demicco, 1982). It consists of inner shelf dolomites and outer shelf limestones. It is a host for hydrocarbons and for Mississippi Valley Type (MVT) mineral deposits. A number of studies, discussed below, have been done on the Romaine Formation since the first investigations of the outcrops in the Mingan Islands where exceptional preservation reveals thrombolite mounds in three dimensions, and later exploratory wells on Anticosti Island. This is, however, the first study to integrate surface-subsurface facies analysis (sedimentology, sequence stratigraphy) with diagenetic investigations (petrography and stable isotope geochemistry) to establish a current framework for the Romaine Formation in the western Anticosti Basin.

PREVIOUS WORK

Geologic Setting

The flooding of the Laurentian margin was most extensive during the middle Early Ordovician (James and Stevens, 1982; James *et al.*, 1988; Williams *et al.*, 1999), the time when the Romaine Formation of the western Anticosti Basin was deposited (Desrochers, 1985, 1988; Pratt and James, 1986). The ancient continental margin has an angular profile

of promontories and reentrants inherited from the rifting that initiated the opening of the Iapetus Ocean (Fig. 1), a profile characteristic of young, thin, hot continental crust (Thomas, 1977; Read, 1989). Margin deposits are thinner on the promontories, St. Lawrence, New York, Virginia, Alabama and Texas Promontories, and thicker on the embayments, the Newfoundland, Quebec, Pennsylvania and Tennessee Embayments (Kesler, 1996). Deposits on the promontories thicken basinward (Pratt and James, 1986; James *et al.*, 1989). Lower Ordovician lithofacies of the continental platform consist of cyclic peritidal carbonates and subtidal carbonates, which are pervasively dolomitized on the inner shelf and partially dolomitized on the mid- to outer shelf respectively (Harris, 1973; Demicco, 1982; James *et al.*,1989). The Anticosti Basin is situated on the St. Lawrence Promontory. The Romaine Formation is buried under lower Paleozoic sediments for the most part. It is exposed in outcrops in the Mingan Islands. Coeval units are the St. George Group of Western Newfoundland (James and Stevens, 1982; Desrochers, 1985; Pratt and James, 1986; Knight *et al.*, 1991); the Beekmantown Group of the St. Lawrence Platform of Quebec and upstate New York (Bernstein, 1992; Friedman, 1994; Lavoie, 1994; Kolkas and Friedman, 1998), the Upper Knox Group of Tennessee (Churnet and Misra, 1981; Montañez, 1992, 1994, 1997; Lumsden and Caudle, 2001); the Arbuckle Formation of Oklahoma (Lindsay and Koskelin, 1991; Gao *et al.*, 1992), and the Ellenburger Group of west Texas (Kerans, 1989; Holtz and Kerans, 1992; Kupecz and Land, 1994). At the onset of the Taconic Orogeny in the Early Middle Ordovician, deposition on the passive margin ceased. During the Taconic orogeny the St. Lawrence Platform was uplifted, faulted and deformed, most intensely at the platform edge. Original fabrics were affected by changes in fluid temperature, pressure and

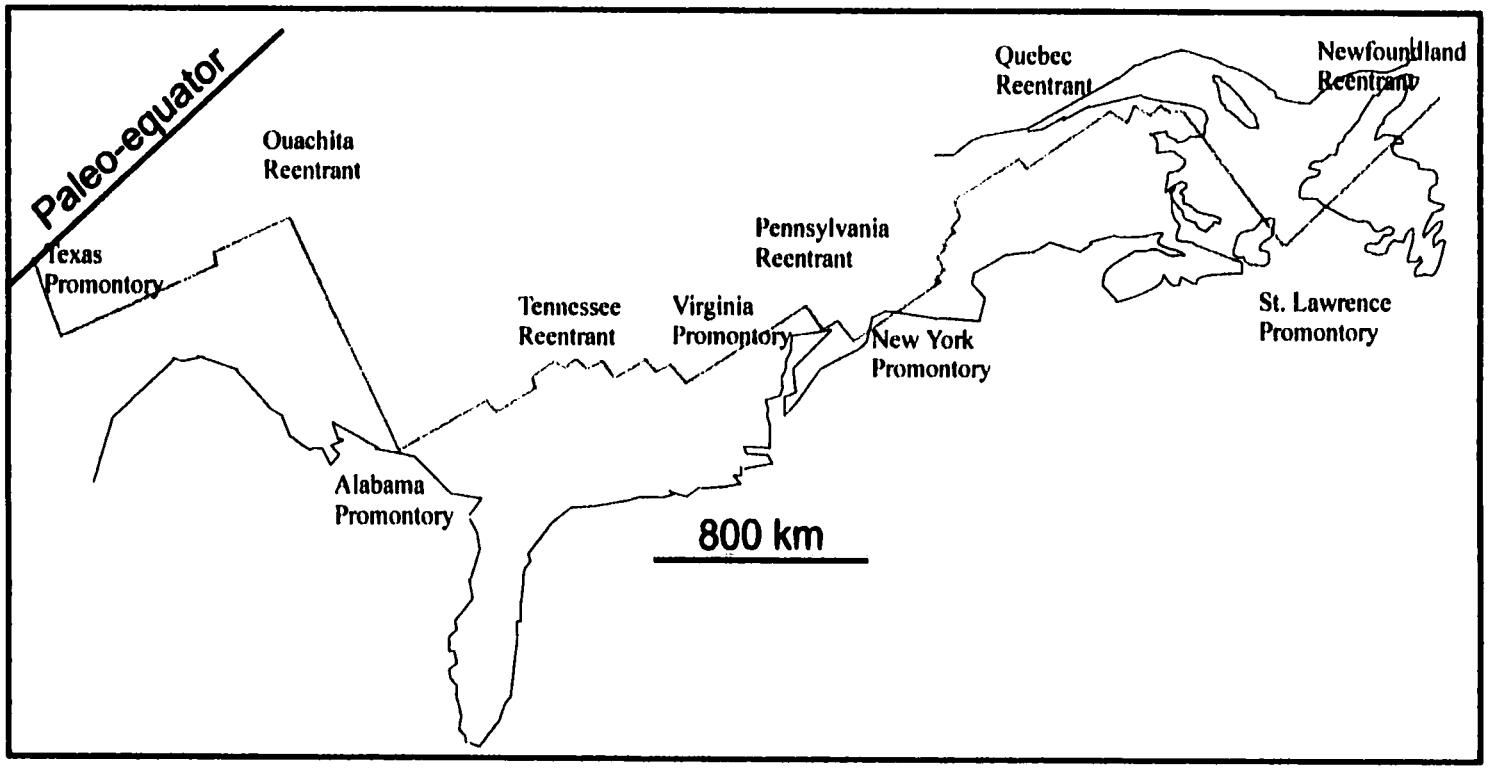

Figure 1. Lower Paleozoic continental margin of eastern North America showing the location of promontories, reentrants and paleoequator (after Harris, 1977; Lavoie, 1994).

chemistry resulting from movement of the peripheral bulge, loading of thrust sheets and burial as a foreland basin developed. These tectonic events resulted in karsting during uplift (Desrochers, 1988); compaction and fluid movement along faults and into porous zones during tectonic thrusting and burial (Montanez, 1992; Davies, 2000; Lynch, 2001). Hydrocarbons and some Mississippi Valley Type (MVT) minerals were emplaced, perhaps as late as the Acadian orogeny (Kesler, 1996). This process was repeated with variations along the continental margin as the Iapetus closed, and several units of the Lower Ordovician margin are host to economic deposits. The Upper Knox Group, the Ellenberger Group and the Arbuckle Formations are hydrocarbon reservoirs. The Upper Knox Group in Tennessee is host to world-class MVT deposits. In Western Newfoundland the St. George Group hosts hydrocarbons (Cooper *et al.*, 2001). MVT deposits have been mined at Daniel's Harbour, Newfoundland (Haywick and James, 1984; Knight and James, 1988; Lane, 1990; Kesler, 1996). The Beekmantown Group of the St. Lawrence Lowlands in the Quebec reentrant has small hydrocarbon reserves to date (Dykstra and Longman, 1994). There is minor mineralization in the Ottawa area, but no significant MVT deposits are known. (Fortin, 1987; Dix *et al.*, 1998). Recent exploration on Anticosti Island resulted in as yet unexploited prospects (Lynch, 2001).

Biostratigraphy

Lower Ordovician Romaine Formation is exposed along 85 km of outcrop in the Mingan Island area. It subcrops in wells on Anticosti Island (Soquip, 1983; Roksandic and Granger, 1981; Desrochers, 1985; Bertrand 1987, 1990) (Fig. 2). The Romaine Formation was deposited on Precambrian basement in the western part of the Anticosti Basin of the St. Lawrence Platform. Biostratigraphy based on brachiopods (Cooper,

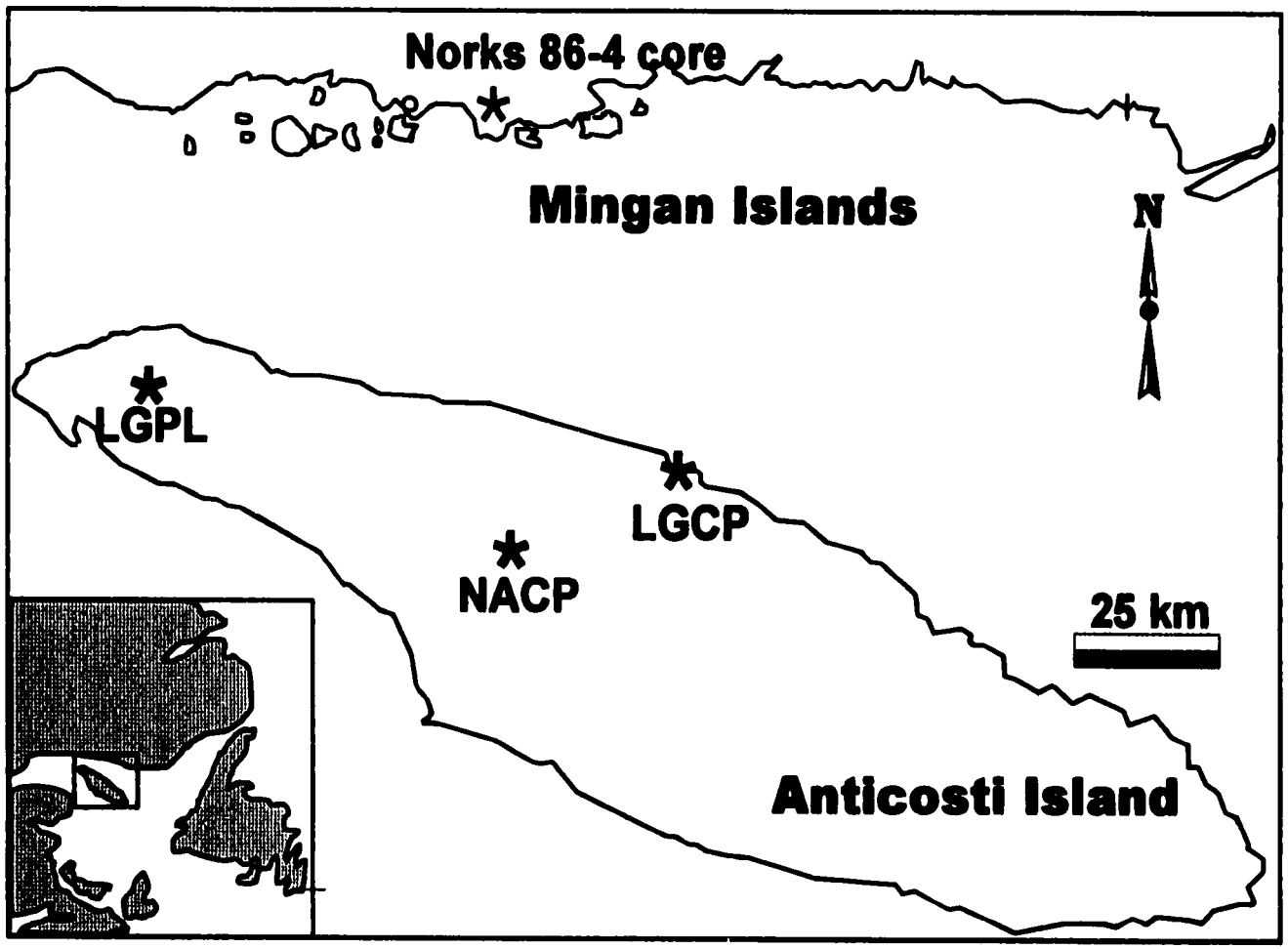

Figure 2. Map of study area showing locations of Anticosti drill cores, Norks core 86-4 and Mingan outcrop belt. Inset map of the Gulf of St. Lawrence.

1956) and on trilobites (Shaw, 1980) refined Early Ordovician dates established by Twenhofel (1938). Bolton (1970b) reported Ordovician fauna in the subsurface of Anticosti Island. Nowlan (1981) investigated conodont biostratigraphy in the area and found that most of the Romaine Formation dated from Late Canadian (Ibexian) time but reported conodonts of Early Whiterockian age at the top of the Romaine Formation in the western Mingan Islands. Desrochers' work (1983, 1984, 1985, 1988) on the Romaine Formation in the Mingan Islands confirmed previous age dating of the formation by macrofossil and conodont data. The Romaine Formation in Anticosti and Mingan is facies-equivalent, and generally time-equivalent to the outer platform Upper Boat Harbour, Catoche and Aguathuna Formations of the St. George Group in Western Newfoundland (Desrochers, 1985, 1988; James *et al.*, 1989; Lavoie, 1994) (Fig. 3).

Facies

In the Mingan Islands, the Romaine Formation is composed of three assemblages of genetically related lithofacies, defined as Members by Desrochers (1983, 1984, 1985, 1988): a basal siliciclastic unit (the Sauvage Member) which grades into the sucrosic, subtidal dolomites of the Sainte-Geneviève Member. The sequence shallows up into the fine-grained dolomites of cyclic peritidal facies of the Grande Île Member. The western outcrops of the Romaine have up to 5 metres of thin bedded subtidal facies at the top, which is truncated by a regional unconformity (Desrochers, 1988; Knight *et al.*, 1991). In the outer platform, the St. George Group is composed of three formations equivalent in age to the Romaine Formation (Knight and James, 1988; Desrochers, 1988), which are the Boat Harbour Formation above the Boat Harbour disconformity (Pratt and James, 1986) also known as the Pebble Bed disconformity (Haywick, 1984), the Catoche Formation,

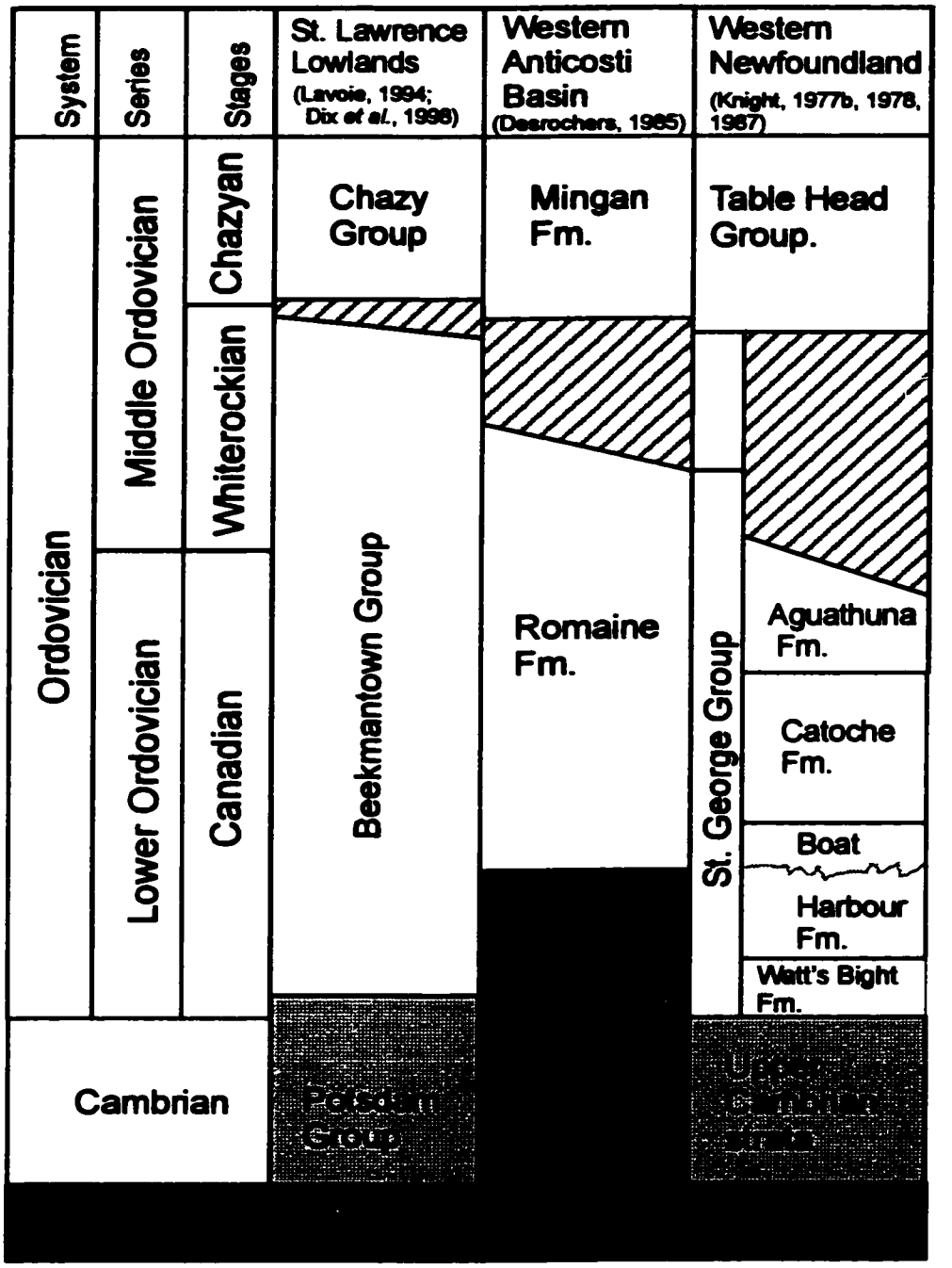

Figure 3. Stratigraphy of the Anticosti Basin and adjacent basins.

and the Aguathuna Formation, which is truncated by the regional St. George unconformity, an unconformity that marks the Sauk-Tippecanoe sequences boundary (Knight *et al.*, 1991).

Fabrics

Carbonate fabrics reflect their depositional and early diagenetic environments. They record the changing temperature, pressure and chemical regimes of burial, uplift and exposure to fluid flow. In the case of dolomite, crystal size and shape reflect the temperature, pressure and degree of supersaturation of fluids of the crystallization environment (Sibley and Gregg, 1987; Warren, 2000). For the Beekmantown Group and the Upper Knox Group, the replacement dolomites of the peritidal facies assemblage are very fine- to fine-grained; subtidal replacement dolomites are generally medium to coarse in crystal size (Lumsden and Caudle, 2001). Cements may be very coarsely crystalline. The same general size categories hold true for the dolomites of the Romaine Formation (Desrochers, 1985; Chi and Lavoie, 2001) and for St. George Group (Haywick, 1984; Lane, 1990).

The Romaine sediments in the Mingan Islands reflect nearshore facies on the St. Lawrence Promontory (Desrochers, 1985; James and Stevens, 1982; James *et al.*, 1988). With the onset of the Taconic orogeny, platform rocks were affected differentially according to their proximity to the orogeny. The outer platform St. George Group was faulted; separate blocks were uplifted or subsided differently as the Taconic orogeny progressed (Knight and James, 1988; James *et al.*, 1988; Stenzel and James, 1990; Knight *et al.*, 1991; Lavoie, 1994). Deformation decreased from the outer margin towards the craton, perpendicular to the facies belts (Desrochers, 1988). Roksandic and Granger

(1981) reported few block faults and folds in the subsurface of Anticosti Island, but later seismic studies indicate block faults trending east-northeast in the western Anticosti Basin (Lavoie, pers. comm.; Chi and Lavoie, 2001; Lynch, 2001; Morin, 2001). The Romaine strata in the Mingan Islands were uplifted, karsted and tilted to the south-southwest (Desrochers, 1985, 1988). The Romaine unconformity is a paleokarst plain truncating progressively older beds to the east. It is estimated that <30 m of section was removed in the easternmost localities of the Mingan Islands (Desrochers, 1985). The platform foundered and the Taconic Foreland Basin developed and accumulated sediments (Knight, 1987, James *et al.*, 1988; Knight *et al.*, 1991; Lavoie, 1994). Estimates of maximum depth of burial based on organic matter reflectance are from 3.3 km in the southwest of Anticosti Island to 4.5 km in the Mingan Islands. Burial temperatures (based on organic matter reflectance) ranged from 115° to 147°C for the three Anticosti wells of this study (Bertrand, 1990). The National Associated Consolidated Paper (NACP) and Lowlands Gamache Carleton Point (LGCP) wells were in the oil window from the late Silurian and moved into the gas condensates zone at later times with uplift (Bertrand, 1990). Recent studies based on fluid inclusions gave temperatures of 131.3° to 137.1°C for the Romaine Formation in Anticosti cores (Chi and Lavoie, 2001).

Isotopes and Fluid Inclusions

Stable oxygen and carbon isotopes have been utilized by previous workers to provide clues for temperature of formation, origin of dolomite, evidence of meteoric or biogenic influences. For the time-equivalent St. George Group, Haywick (1984) and Lane (1990) reported isotope results for $\delta^{18}O$ and $\delta^{13}C$ in dolomite and calcite fabrics that are more negative than Lower Ordovician seawater according to Lohmann (1989). Chi and

Lavoie (2001) reported values for the Romaine Formation that were more negative than expected for Lower Ordovician seawater. Values reported by the above workers for Lower Ordovician units of the St. Lawrence Platform are generally similar to values reported for the Upper Knox Group (Montañez, 1992, 1994), the Ellenberger Group (Kupecz *et al.*1993; Kupecz and Land, 1994), and the Arbuckle Group (Gao, 1990). Fluid inclusion analyses are used in conjunction with stable isotope results to assign temperatures of dolomite precipitation or recrystallization and help to constrain the nature of diagenetic fabrics. Fluid inclusion results reported for the Romaine are equivocal in terms of assigning a burial or hydrothermal origin to late dolomitization and MVT mineralization (Lavoie *et al.*, 2000; Chi and Lavoie, 2001). This is also true for the Upper Knox Group MVT and hydrocarbon deposits (Lumsden and Caudle, 2001). Because peak temperature is reached before cement deposition ends, Chi and Lavoie (2001) propose a significant hydrothermal event to account for late carbonate cements in the Romaine Formation.

MATERIALS AND METHODS

The Romaine section was studied in three cores from the subsurface Anticosti Island, Lowlands Gamache Princeton Lake (LGPL), New Associated Consolidated Paper (NACP) and Lowlands Gamache Carleton Point cores (LGCP) (Fig. 3). A. Desrochers provided logs from 5 onshore cores, Norks cores 86-1, 86-2, 86-3, 86-4 and 86-5 (Fig. 3). The core logs provided continuous data on lithology, sedimentary structures, and porosity; and facies assemblages were interpreted from this data. 453 thin sections (112 from samples of the three Anticosti Island cores; 97 from samples of the Norks cores and a set

of 244 stained thin sections from outcrops of the Romaine Formation) provided data on mineralogy, dolomite types, cements, accessory minerals and microscopic relations between mineral phases.

All thin sections were stained with a solution of Alazarin Red-S to evaluate the distribution of calcite and dolomite and Potassium Ferricyanide to test for ferroan carbonate according to the Dickson method (Dickson, 1966). Thin sections for ordinary light microscopy were covered with a cover slip. They were examined under plane, polarized and under diffuse light using the white card technique (Dravis, 1990).

Thirty-eight thin sections for cathodoluminescence were doubly polished, unstained and uncovered. A Technosyn model cathodoluminoscope was used. Usual working conditions were 15-20 Kv and 530-580 μA for an unfocussed electron beam.

Dolomite crystals and fabrics were classified according to Sibley and Greg's scheme (Sibley and Greg, 1987). Where it was difficult to distinguish between planar-subhedral and nonplanar-anhedral fabrics, a count of 100-300 crystals across a traverse was made to determine if more or less than 30% of crystals had crystal face junctions (Greg and Sibley, 1984). Fine-grained dolomite fabrics were examined under 200X magnification to determine exactly where the characteristic blue colour stain for iron was situated. Where the fabric of crystals was blue, the dolomite was classed as ferroan dolomite. Where blue stain was restricted to cements infilling earlier intercrystalline porosity and damaged or eroded portions of the crystal, the earlier dolomite was classified as non-ferroan and the later cement was classified as ferroan.

Samples selected for stable isotope analysis after phases were identified and examined by cathodoluminescence microscopy to find out if there were multiple cement

zones to test. For early replacement dolomite, an attempt was made to take samples with the least overprinting of late ferroan dolomite cement, but no sample was entirely free of late ferroan dolomite cement. Stable isotopes of micro-drilled powders of 59 calcite and dolomite samples were analysed at the G.G. Hatch Isotope Laboratories at the University of Ottawa. The carbon and oxygen isotopic composition was determined by the analysis of CO_2 generated by the reaction with 100% phosphoric acid (McCrea, 1950). The $\delta^{18}O$ fractionation factors used for the carbonate-H_3PO_4 reactions were

calcite at 25°C α=1.01025 (Friedman and O'Neil 1977; Sharma & Clayton 1965)

dolomite at 50°C α=1.01065 (Rosenbaum and Sheppard 1986)

The CO_2 was analysed on a triple collector VG SIRA 12 mass spectrometer. The routine precision on a pure carbonate analysis was 0.10‰ for both carbon and dolomite isotopes. More than twenty samples were selected for fluid inclusion analysis, but as only preliminary results are available at this time, that work will be reported in future studies.

RESULTS

Core and Outcrop Summary

Data from three cores from Anticosti Island, one core from the Mingan Islands and from the Mingan Islands outcrop belt are summarized in Figures 4 to 9, showing facies assemblages, sample depths, lithology and sedimentary features in the first column, dolomite types in the second column, porosity in the third column, late cements in the fourth column and stable isotope results in the last column. All data is plotted against

Legend

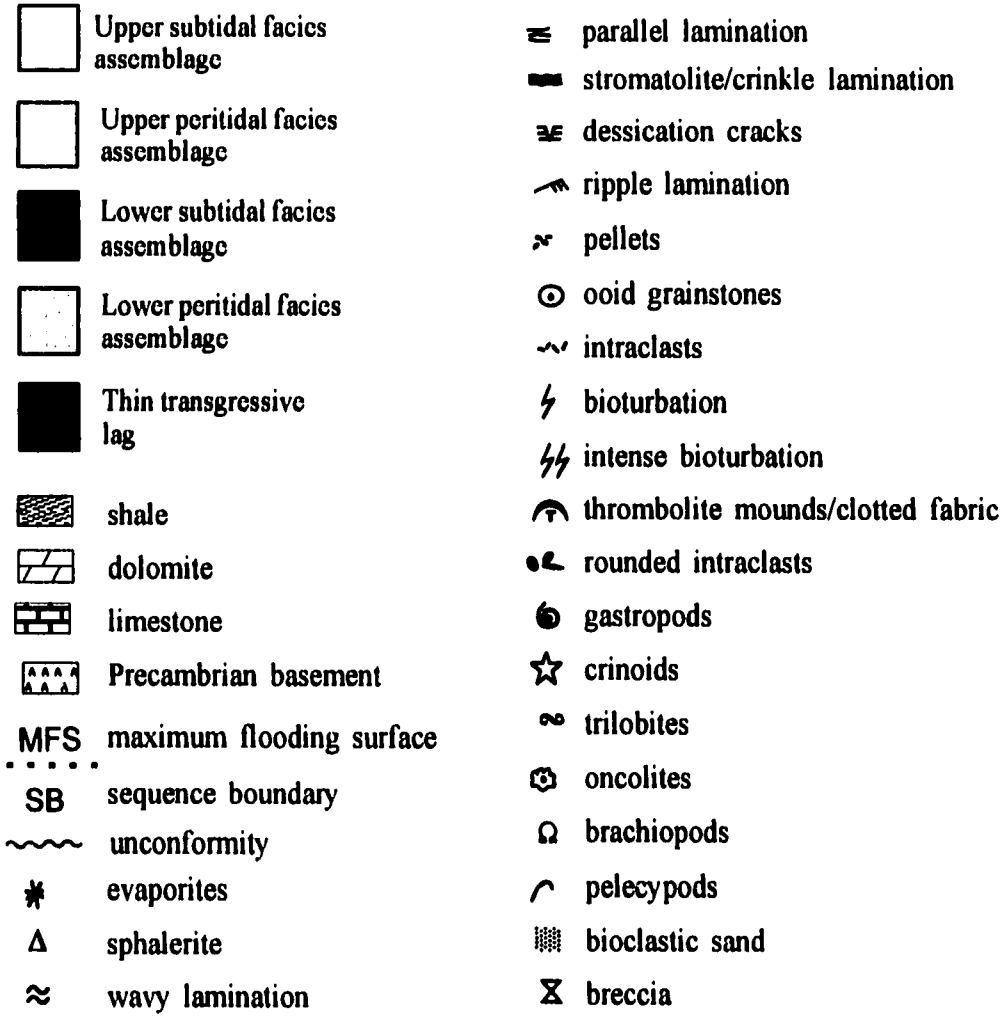

Figure 4. General legend for figures 5-8 and 21-23.

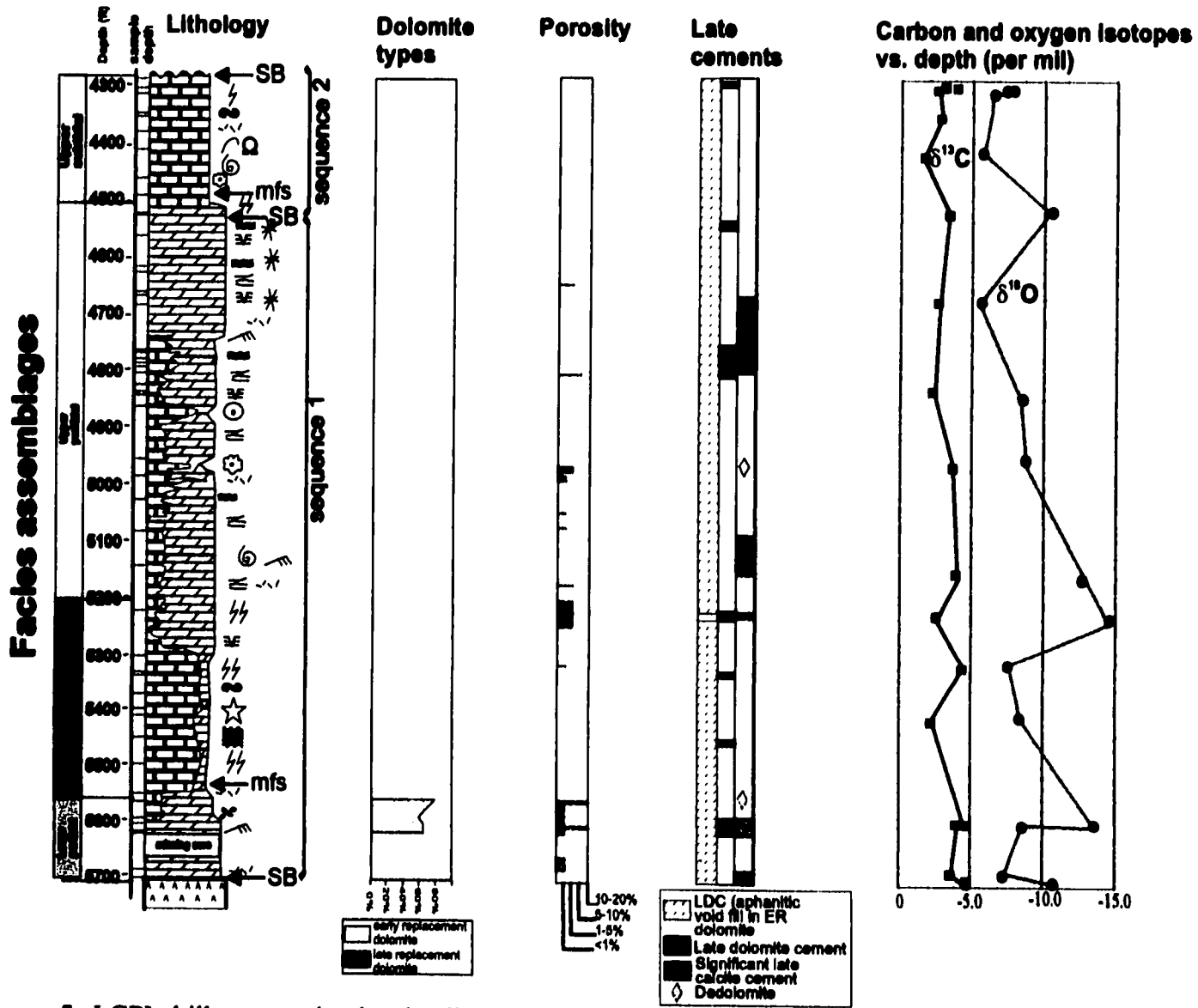

Figure 5. LGPL drill core results showing lithofacies, facies assemblages, sequences, dolomite types, porosity, late cements and stable isotope results.

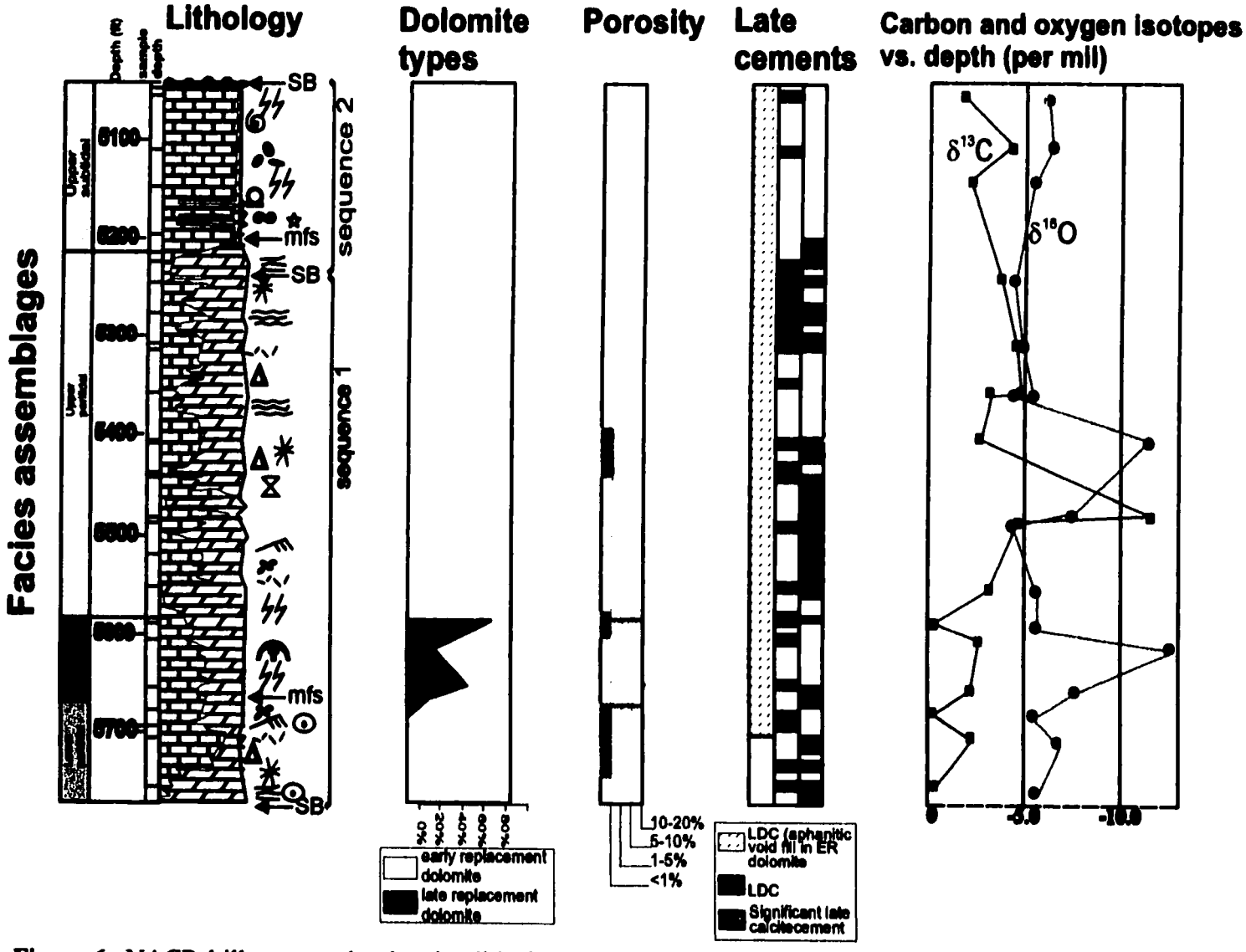

Figure 6. NACP drill core results showing lithofacies, facies assemblages, sequences, dolomite types, porosity, late cements and stable isotope results.

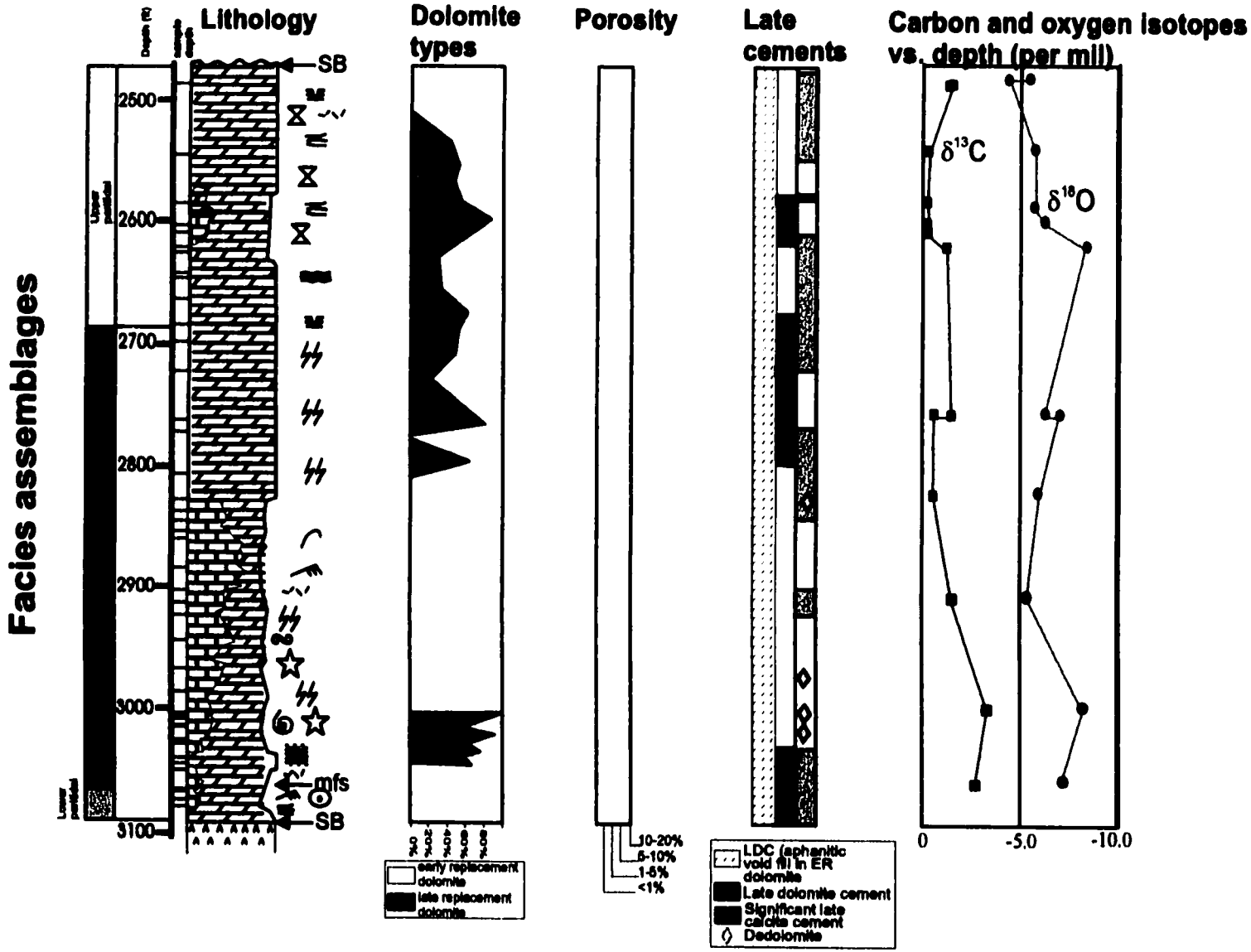

Figure 7. LGCP drill core results showing lithofacies, facies assemblages, dolomite types, porosity, late cements and stable isotope results.

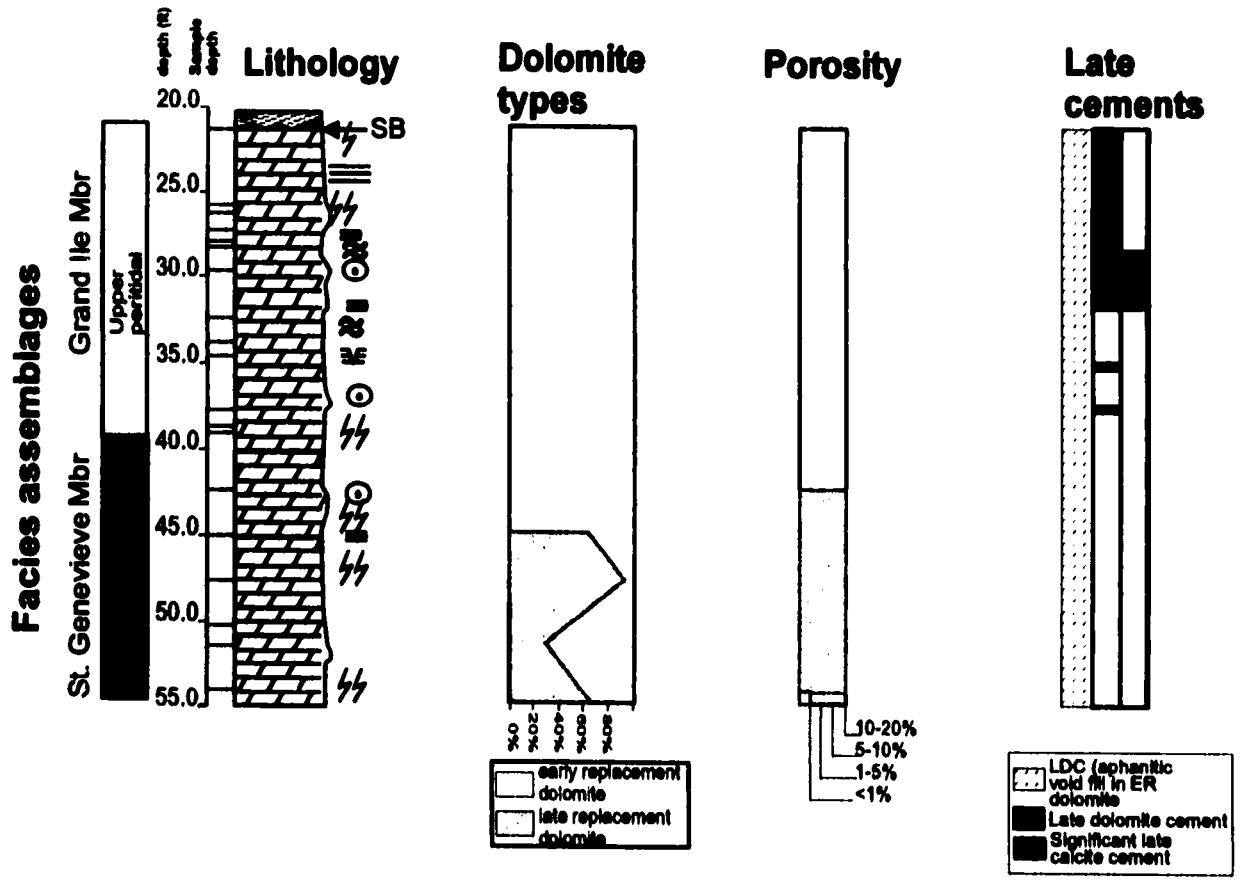

Figure 8. Norks 86-4 drill core results showing lithofacies, facies assemblages, dolomite types, porosity and late cements.

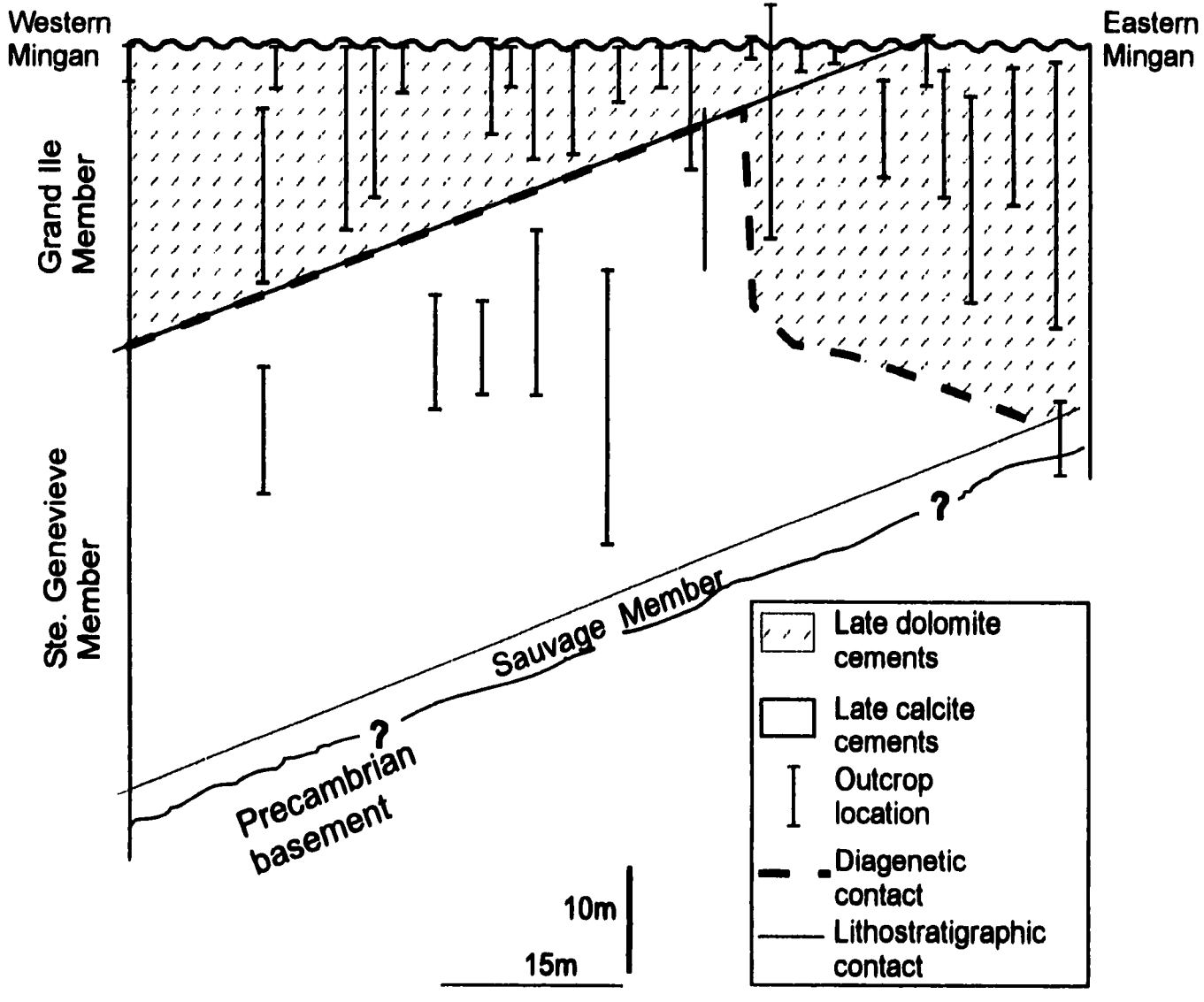

Figure 9. Romaine Formation in the Mingan Outcrops showing the distribution of late cements (after Desrochers, 1985).

depth. Data for dolomite types is quantitative only at sample locations. Data for late cements is not quantitative. Figure 4 shows the legend for Figures 5-8.

Figure 5 is a graphic summary of well-log and thin section data from the Lowlands Gamache Princeton Lake Core (LGPL), the westernmost of the drill cores logged. The well penetrates 1412 feet (430 m) of Romaine Formation rock to Precambrian gneiss at a depth of 5707 feet. Porosity is not significant in LGPL. Mississippi Valley Type minerals are not observed in LGPL (Fig.5).

Data from well-log and thin section analysis of samples from the New Associated Consolidated Paper drill core (NACP) are summarized graphically in Figure 6. NACP is the southernmost of the drill cores logged. It sampled 726.5 feet (221.4 metres) of Romaine Formation rock. Although it does not penetrate Precambrian basement rock, the basement is near the 5770-foot depth (1759 m) of the end of the core (Claude Morin, pers. comm., 2001). Late cements, specifically blocky and poikilotopic calcite cements, make up to 33% of some rock samples. Saddle dolomite and sphalerite are also common in this core. Porosity is not high or extensive in the core. At 5581-5583 feet depth (1701-1702 m), drillers made the notation "brown oil bleeding from core".

Figure 7 summarizes well log and thin section data from the Lowlands Gamache Carleton Point well (LGCP), the easternmost of the drill cores studied. It samples 607.9 feet (185.3 metres) of the Romaine Formation. Precambrian basement is penetrated at a depth of 3092 feet (943 m). An interval of dissolution-collapse breccia is observed between depths of 2620 ft. and 2500ft (799-762 m). The breccia clasts increase in size upwards. There is significant porosity (<20%) in portions of the brecciated interval.

Of five cores available from onshore quarries (Norks cores 86-1, 86-2, 86-3, 86-4,

86-5), Norks core 86-4 is depicted as a representative of the other 4 cores, all of which are located east of 86-4 on Grande Pointe. Figure 8 is a graphic summary of well-log and thin section data from this core. Norks core 86-4 samples 30.8 m (101 feet) of Romaine strata. It does not penetrate the Precambrian basement. Green coloured shales are observed near the Romaine-Mingan contact, forming shaly partings at 34 ft. (10.4 m) and 35 ft. (10.7 m). Green clay is observed in vugs at 66 ft. depth (20 m). Vuggy porosity is observed associated with high percentages of late replacement dolomite (Fig. 8).

In the Mingan Islands about 85 km of outcrop expose the Romaine Formation (Desrochers, 1985). The thin section suite examined in this study samples the Romaine Formation over the whole span of the outcrops, providing the northernmost dataset on the formation. Data from the thin sections is summarized in Figure 9. The Romaine Formation is pervasively dolomitized throughout the Mingan Islands. Locally clumps of sponge spicules are observed. Compacted rhomb prisms occur in the western part of the Ste. Genevieve Member, but are not observed elsewhere in the Mingan Islands thin section suite. Calcite and silica cements are ubiquitous.

Lithofacies

The Romaine peritidal and subtidal carbonates comprise seven distinct lithofacies in core and outcrop, grouped into two carbonate facies assemblages. An eighth lithofacies (the Sauvage Member), a feldspathic sandstone is the basal transgressive unit in the Mingan Islands. These lithofacies were defined in pervasively dolomitized outcrops in the Mingan Islands where preservation/weathering has made it possible to document structures in megascopic, three-dimensional detail (Desrochers, 1983, 1984a, 1985, 1988). Table 1 summarizes the 8 lithofacies found in the Mingan Islands outcrops and Norks

Table 1. Summary of facies assemblages of the Romaine Formation (After Desrochers, 1988)

Facies assemblage	Lithofacies name	Lithology	Depositional environment	Distribution
Peritidal facies assemblage	A-feldspathic sands	20-30% feldspar; mature texture; cross stratified; restricted marine fauna; *Skolithos*	Littoral sand belt	Basal assemblage in Mingan outcrops; poorly preserved with poor recovery in Anticosti cores
	B-Dololaminites	Parallel and wavy laminated; desiccation cracks; teepee structures; flat pebble conglomerates, evaporites	Supratidal Sabkha	Near top of upper peritidal cycles in both cores and outcrops
	C-Ripple laminated dolomicrites	Current laminations; parallel, wavy and lenticular bedding; rare desiccation cracks	Mixed intertidal flats	Middle part of peritidal facies cycles in both cores and outcrops
	D-Stromatolitic dolomicrite	LLH stromatolites; desiccation cracks; digitate stromatolites, crinkled laminae	Intertidal zone	Middle part of peritidal facies cycles in both cores and outcrops
	E-Lagoonal dolomicrites	Moderate to intense bioturbation; restricted marine fauna, pellets	Semi-restricted lagoon	Base of some peritidal lithofacies cycles in outcrops and Norks cores
	F-Ooid dolograinstones	Massive to laminated unit; medium sand grain-size; well-sorted; radial or concentric cortices	Oolitic sand belts	Base of some peritidal lithofacies cycles in outcrops and Norks cores
Subtidal facies assemblage	G-Subtidal bioturbated	Intensely bioturbated (mostly *Palaeophycus*); intraclast layers (tempestites); diverse fauna, calcarentite tempestites	Open circulation outer shelf	Inter mound facies in outcrops and onshore cores; dominant lithofacies in subtidal intervals in Anticosti cores
	H-Thrombolite facies	Thrombolite mounds, 1-3 m, joined or isolated; adjacent intraclast beds; clotted fabric	Shelf patch reefs and associated diverse fauna	Upper part of lower subtidal assemblage in outcrop, Possibly present in cores, but difficult to recognize clotted fabric

cores and in the three Anticosti Island cores. The peritidal facies assemblage includes five lithofacies, 1) sabkha/supratidal dololaminate (Fig.10b), 2) intertidal, ripple laminated dolomicrites (Fig. 10c), 3) intertidal stromatolitic dolomicrites (Fig. 10d), 4) lagoonal, bioturbated dolomicrites (Fig. 11a), and 5) sand shoal, ooid dolograinstones (Fig. 11b). The open marine, subtidal facies assemblage includes two lithofacies, 1) thin, intensely burrowed skeletal and intraclastic mudstones, wackestones and packstones (Fig. 11c) with tempestite beds, and 2) thick thrombolitic beds which interfinger with the thin, burrowed beds bearing a diverse fossil fauna (Figs. 11d and 12a) and rounded intraclasts (Fig. 12b). The peritidal and subtidal carbonate lithofacies are observed in outcrop, in the five cores from the Mingan area and in the three cores from Anticosti Island (Figs. 5-9). The two assemblages of carbonate lithofacies show differences in lithofacies abundance and distribution between the inner shelf Mingan sections and the mid-shelf Anticosti cores. In the Anticosti cores, cyclic peritidal units are pervasively dolomitized, but subtidal units are partially dolomitized. The three Anticosti Island cores penetrate a thin, discontinuous transgressive lag at the base, however, the cores are rubbly near the contact with the Precambrian basement and recovery is very poor. Typically, thin sections from the base of the cores contain intraclasts from peritidal facies, burrowed sandy dolomites, and abundant siliciclastic shales (Fig. 10a). The contact between these initial deposits to cyclic peritidal facies is gradational. An assemblage of subtidal facies similar to the dolomitized Ste. Genevieve Member overlies the peritidal facies assemblage in all three Anticosti Island cores, but again, the subtidal facies are only partially dolomitized in LGPL, NACP and LGCP. Overlying the subtidal unit is a second peritidal unit similar to the Grand Ile Member in the Mingan section. Evaporites and pseudomorphs of evaporates are observed

Figure 10

Photomicrographs of lithofacies in Anticosti Island cores

(Plane polarized light)

A. Thin section photomicrograph showing poorly sorted, angular to round quartz and feldspar grains in a fine to medium crystalline dolomite matrix. Scale bar is 500 μm. Sample source is LGPL core at 5707 ft. depth (1739 m).

B. Thin section photomicrograph of dololaminite showing very finely crystalline dolomite laminae with anhydrite layer. Scale bar is 100 μm. Sample source is LGPL core at 4630 ft. depth (1411.6 m).

C. Thin section photomicrograph of rippled dolomite showing ripple cross-laminated dolomicrites. The ripple has a sharp base and diffuse top. Larger, lighter coloured dolomite in the ripple contrasts with dark, structureless dolomicrites below. Scale bar is 3 mm. Sample source is NACP core at 5550 ft. depth (1692 m).

D. Thin section photomicrograph of dark, stromatolitic, crinkled laminae with layers of fine to medium crystalline, lighter coloured dolomite Scale bar is 200 μm. Sample source is LGPL core at 4666 ft. depth (1422.6 m).

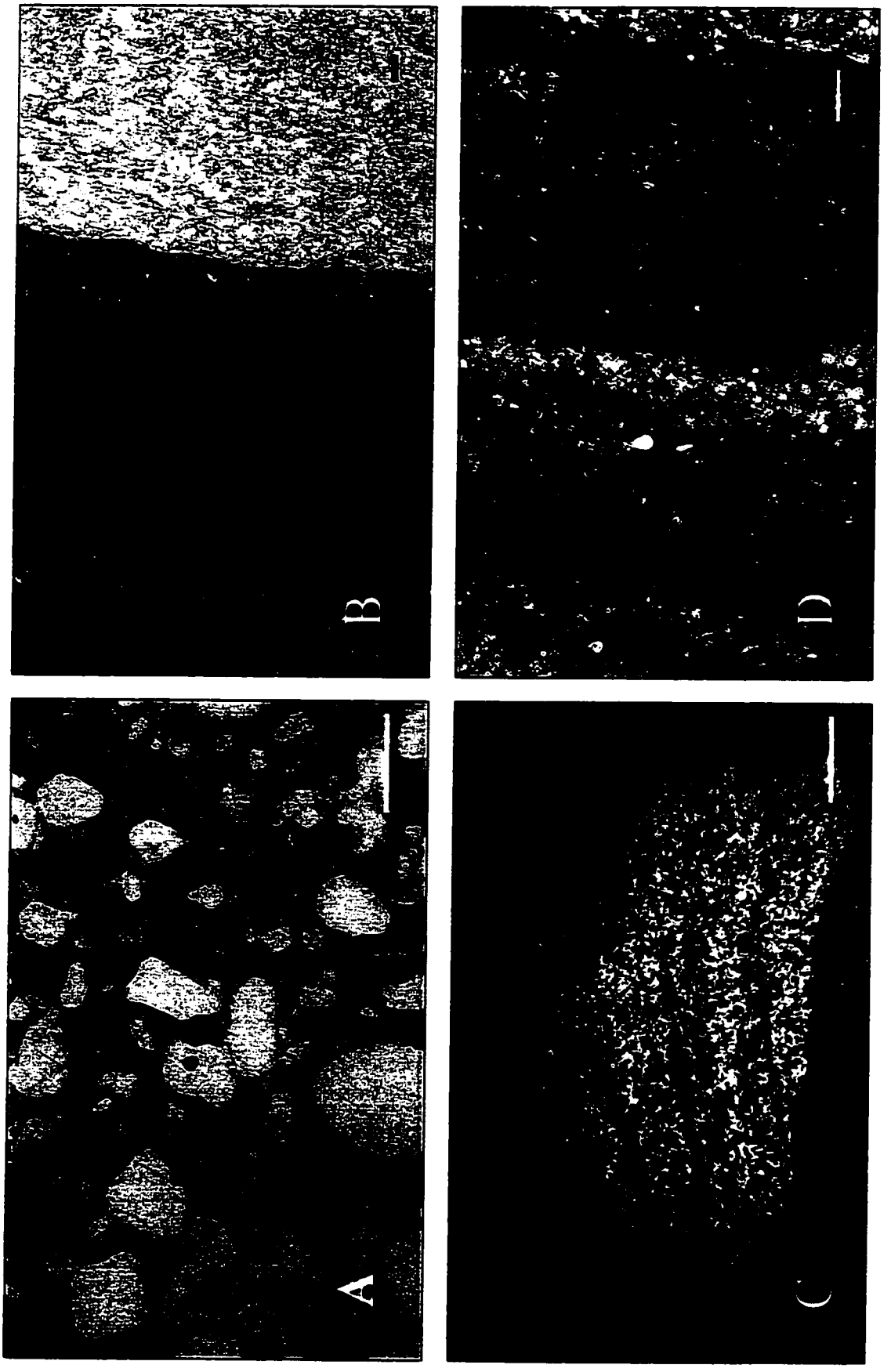
B
D
A
C

Figure 11

Photomicrographs of lithofacies in Anticosti Island cores

(Plane polarized light)

A. Thin section photomicrograph (plane polarized light) of lagoonal dolomicrite with pellets and burrows (dark, very fine grained dolomite). Scale bar is 1.2 mm. Sample source is NACP core at 5314 ft. depth (1620 m).

B. Thin section photomicrograph of ooid dolo-grainstone. Note very finely crystalline ooid rims and cores, and poikiltopic calcite cement. Scale bar is 600 μm. Sample source is LGPL core at 4827 ft. depth (1471.6 m).

C. Thin section photomicrograph of bioturbated subtidal facies showing burrowed lime micrite. Burrows are light coloured, fine to medium crystalline dolomite. Scale bar is 700 μm. Sample source is LGPL core at 5331 ft. depth (1625 m).

D. Thin section photomicrograph subtidal facies (upper subtidal) showing bioclastic wackestone. Note dolomitized burrow at the right of the image. Scale bar is 400 μm. Sample source is LGPL core at 4388 ft. depth (1337.8 m).

A
B
C
D

Figure 12

Photomicrographs of lithofacies in Anticosti Island cores

(Plane polarized light)

A. Thin section photomicrograph upper subtidal facies showing bioclastic wackestone with trilobite, brachiopod and crinoid fragments in lime micrite. Scale bar is 500 μm. Sample source is LGPL core at 4356 ft. depth (1328 m).

B. Thin section photomicrograph of lower subtidal facies showing rounded intraclasts and fossil debris in lime micrite. The large recrystallized shell at the top of the image is part of a high-turretted gastropod. Scale bar is 550 μm. Sample source is LGCP core at 4827 ft. depth (1471.6 m).

C. Thin section photomicrograph of upper subtidal facies showing lime micrite. Late calcite cement occludes porosity. Scale bar is 240 μm. Sample source is NACP core at 5222 ft. depth (1592 m).

D. Thin section photomicrograph of upper subtidal facies showing oncolite (*Girvanella*). Scale bar is 8 mm. Sample source is LGPL core at 4497 ft. depth (1371 m).

A
B
D

near the top of this upper peritidal unit in the Anticosti cores. In the westernmost cores, LGPL and NACP, a second subtidal unit occurs, similar to the upper five metres of "lagoonal" lithofacies of the Grand Île Member in western outcrops (Figs. 5 and 6). The upper subtidal unit is largely muddy limestone in Anticosti cores (Fig. 12c). The upper assemblage of subtidal facies is dissimilar to the lower subtidal facies assemblage as follows: 1)thrombolite textures are absent, 2) little dolomitization is present in the two Anticosti Island cores, LGPL and NACP, and 3) the presence of calcite pseudomorphs of gypsum, and oncolites (Fig. 12d) may indicate either near shore lagoonal or shelfal subtidal environments.

Dolomite Fabrics

Sedimentary dolomite fabrics or textures are the basis for classifying replacement dolomites according to Sibley and Gregg`s system (1987). Textures vary in response to differences in temperature and pressure regimes and to differences in fluid supersaturation with respect to dolomite. Dolomite fabrics are distinguished based on petrography (light, diffuse light and cathodoluminescence). Crystal size distribution (unimodal or polymodal) and shape (planar boundaries or nonplanar boundaries) are the principle textural attributes that reflect response to dolomitizing environment. Crystal size distribution is polymodal in the Romaine Formation; even at the scale of the thin section scale, unimodal size distribution is rare. Crystal shape, the second attribute reflecting response to dolomitizing fluid, is classified as by whether the crystal has planar or nonplanar boundaries. Planar boundaries may be planar crystal faces or compromise boundaries between crystals. Crystals with planar boundaries, belong, with few exceptions, to the very fine (4 μm to16 μm), fine (16 μm to 62 μm) to medium (62 μm to 250 μm) crystal size range. Crystals

with nonplanar boundaries include those with lobed, serrated, curved, or otherwise irregular boundaries (Sibley and Gregg, 1987). In the Romaine Formation, replacement dolomite with nonplanar boundaries is, with few exceptions in the medium to coarse (250 μm to 1mm) size range.

The Sibley and Gregg (1987) classification system further describes dolomite textures in terms of type of replacement of matrix, allochems and early cements. In the Romaine Formation, replacement differs depending on the extent of dolomitization. In intervals composed of dolomite (90-100% dolomite) and calcitic dolomite (50-90% dolomite) the matrix is replaced. Most originally calcite or aragonite allochems are present as molds filled with late cements or are non-mimetically replaced. In rare cases, allochems are not replaced. Early calcite cements are replaced non-mimetically, or rarely, replaced mimetically. It should be noted that the calcite content of dolomite and calcitic dolomite intervals is late calcite void and fracture-fill cement; it is not sedimentary or early marine calcite.

In limestone (0-10% dolomite) and dolomitic limestone (10-50% dolomite) the matrix is typically unreplaced or partially replaced by a few individual rhombs or patches of planar-e to planar-s dolomite. The allochems are partially or completely replaced by very fine to medium grained dolomite. No instances of mimetic replacement by dolomite are present in limestone or dolomitic limestone. In limestone and dolomitic limestone, early calcite cements are not replaced or partially replaced by dolomite.

Planar bounded, very fine to medium grained, replacive dolomite textures as described above, are generally considered early dolomite textures (Haywick, 1984; Desrochers, 1985, 1988; Lane, 1990). They are the dominant phase of dolomite in the

study area. Nonplanar replacement dolomite is considered a late and/or high temperature replacive dolomite (Gregg and Sibley, 1984; Sibley and Gregg, 1987; Warren, 2000). Planar dolomites in the Romaine Formation are divided into two sub-categories distinguished on the basis of general crystal size and depositional environment: 1) very fine to fine-grained early replacement dolomite that dominates peritidal facies (ER1), and 2) fine to medium-grained early replacement that is the dominant dolomite in subtidal facies (ER2). Nonplanar dolomite is medium to coarse-grained and makes up the single category of late replacement dolomite (LR). Late dolomite cements (LDC) include ferroan and non-ferroan phases in which cement shows parallel extinction or undulose extinction and curved crystal faces. The characteristics of the three replacement and single cement dolomite fabrics are summarized in Table 2.

ER1 dolomite is very fine to fine in size. It has planar boundaries and forms loose mosaics. It is typically a "dirty dolomite"; many rhombs have cloudy inner zones and clear outer zones. Ferroan dolomite cement associated with the ER1 dolomite commonly fills intra-crystalline fractures and dissolution voids and inter-crystalline space (Figs. 13a-d). Distribution of ER1 dolomite is generally restricted to peritidal facies assemblages (Figs. 5-9). Very fine ER1 fabrics are observed in dololaminates, rippled dolomicrites, stromatolitic facies, and as a replacement for micritized parts of allochems in lagoonal and ooid shoal facies. Cathodoluminescence response of ER1 dolomite is dull red luminescence to non-luminescent.

ER2 fabrics are fine to medium in crystal size. They form loose mosaics of planar-e dolomite (Fig. 14a) and dense mosaics of planar-s dolomite (Fig. 14b). Rhombs commonly have cloudy cores and clear outer zones. In planar-e fabrics, cores of rhombs

Table 2. Dolomite fabrics in the Romaine Formation

Textural type	Occurrence	Crystal size	Optical properties	$\delta^{13}C_{(PDB)}$ ‰	$\delta^{18}O_{(PDB)}$ ‰
Planar replacive ER1	Peritidal facies	Very fine to fine 4-62 μm	Cloudy in transmitted light; CL, dark red luminescent or non-luminescent	-0.29 to -4.91‰ Mean = -2.56‰ (n = 19)	-4.43 to -10.79 ‰ Mean = -6.21‰ (n = 19)
Planar replacive ER2	Subtidal facies	Fine to Medium 62-250 μm	Commonly have cloudy cores, clear rims; CL, dark red luminescent or non-luminescent		
Nonplanar replacive LR	Porous limestone & near fractures	Medium to coarse 250 μm – 1mm	Rare undulose extinction; CL, dark red luminescent or non- luminescent	-0.31 to -4.10‰ Mean = -1.32‰ (n = 12)	-4.50 to -8.49 ‰ Mean = -6.52‰ (n = 12)
Void-filling dolomite Cement LDC	Voids and fractures	aphanitic to very coarse	Planar crystal faces/parallel extinction to curved crystal faces/undulatory extinction CL, dark red luminescent or non-luminescent	-0.20 to -4.99‰ Mean = -2.73‰ (n = 7)	-4.43 to -13.79‰ Mean = -8.07‰ (n = 7)

Figure 13

Photomicrographs planar replacement, ER1, dolomite fabrics

(Plane polarized light)

A. Thin section photomicrograph of planar ER1 dolomite replacement of lagoonal micrites showing the very fine to fine crystalline nature of dolomite crystals. Scale bar is 600 μm. Sample source is NACP core at 5314 ft. depth (1620 m).

B. Thin section photomicrograph of planar replacement, ER1 dolomite showing the planar nature of the crystals and the ferroan LDC cement filling submicron intra- and intercrystalline voids. Scale bar is 100 μm. Sample source is LGPL core at 4807 ft. depth (1463.4 m).

C. Thin section photomicrograph of planar ER1 dolomite showing very fine crystalline replacement of ooid rim and core and finely crystalline dolomite replacement of matrix. Scale bar is 500 μm. Sample source is LGPL core at 4839 ft. depth (1475.3 m).

D. Thin section photomicrograph of planar ER1 dolomite showing fine crystalline dolomite replacement of matrix and very fine crystalline replacement of burrows. Note saddle dolomite at edge of dissolution void (under scale bar), and late calcite void fill cement. Scale bar is 300 μm. Sample source is NACP core at 5606 ft. depth (1709.1 m).

A
B
C
D

Figure 14

Photomicrographs planar replacement, ER2, dolomite fabrics

(Plane polarized light)

A. Thin section photomicrograph of planar ER2 dolomite showing medium crystal size, planar-e dolomite at the center and planar-s dolomite around the edges of the image. Scale bar is 70 μm. Sample source is NACP core at 5194 ft. depth (1583.5 m).

B. Thin section photomicrograph of planar-s ER2 dolomite showing the planar nature of the crystals and the ferroan LDC cement filling submicron intra- and intercrystalline voids. Scale bar is 100 μm. Sample source is LGCP core at 2645 ft. depth (806.4 m).

C. Thin section photomicrograph of planar ER2 dolomite showing characteristic dissolution of planar-e rhombs, leaving remnant rims. Note ferroan LDC overprint and small amount of late calcite cement fill. Scale bar is 100 μm. Sample source is Norks core, 86-4 at 39 ft. depth (11.9 m).

D. Thin section photomicrograph of planar ER2 dolomite showing medium crystalline, planar-s dolomite replacement of allochems in packstone. Note slight blue stain indicating slightly ferroan composition of crystals. Scale bar is 225 μm. Sample source is LGCP core at 2982 ft. depth (909.1 m).

A
B
C
D

are frequently dissolved. Locally all but the rims of the rhombs are dissolved (Fig. 14c). In some areas, this dissolution leaves prism-like remnants of the rims of the rhombs. Ferroan dolomite cement commonly fills dissolution voids and fractures in crystals. However, calcite may fill these voids and fractures. In loose mosaics of planar-e, ER2 dolomite, poikilotopic, late calcite cement commonly fills intercrystalline voids. Planar-s dolomite textures form tight mosaics between porous, planar-e dolomite pockets. Planar-s rhombs are not affected by dissolution from the center outward, but sub-micron intra-crystalline voids and fractures are filled with ferroan dolomite (Fig.14b). ER2 is the dominant dolomite fabric in subtidal facies assemblages (Figs. 5-9). Cathodoluminescence response of ER2 dolomite is dull red luminescence to non-luminescent.

Two minor subsets of ER2 dolomite fabric are present. The first occurs as clusters of planar-s rhombs, which replace calcite cements inside allochems in limestone or calcitic matrices (Figs. 14d). These rhombs are commonly slightly ferroan in composition. The second subset of ER2 dolomite fabric consists of fine to medium, planar e- rhombs occurring as individual rhombs "floating" in a fine-grained dolomite or limestone matrix. These are typically concentrated near solution seams and stylolites as described by Wanless (1979) (Fig. 15a).

Of the two late dolomite fabrics LR dolomite is a late replacement fabric and LDC dolomite is a late void and fracture filling cement. LR dolomite is mainly medium to coarsely crystalline. Crystals have nonplanar, irregular boundaries (Fig.15b). This replacement dolomite obliterates the original limestone fabric; but under diffuse light, inclusion-rich zones may outline allochems in the original fabric. LR dolomite, unlike ER dolomite, rarely contains submicron sized fractures or voids filled with ferroan dolomite

Figure 15

Photomicrographs planar replacement, ER2, dolomite fabrics and nonplanar, late replacement, LR, dolomite fabric (Plane polarized light)

A. Thin section photomicrograph of planar ER2 dolomite showing fine to medium crystalline "floating" dolomite rhombs in lime matrix concentrated near solution seam. Scale bar is 100 μm. Sample source is NACP core at 5047 ft. depth (1538.7 m).

B. Thin section photomicrograph of nonplanar LR dolomite showing the irregular boundaries and medium to coarsely crystalline nature of the replacement dolomite. Scale bar is 350 μm. Sample source is Norks core 3-18. at 18 ft. depth (5.5 m).

C. Thin section photomicrograph of brecciated nonplanar LR late replacement dolomite showing solution seams cutting matrix and cutting breccia clast. Note eroded, zoned, planar-e dolomite rhombs in dark matrix. Scale bar is 250 μm. Sample source is an outcrop of the St. Geneviève Member in the western Mingan Islands.

D. Thin section photomicrograph of nonplanar dolomite mimic replacement of early marine calcite cements in ooid-dolograinstone. Note ER1 dolomicrite replacement of replacement of micritic envelope and ooid core, dropped cores, ferroan LDC cement, and late calcite cement fill of voids in ooids. Scale bar is 600 μm. Sample source is Norks core 86-4 at 22 ft. depth (6.7 m).

A
B
C
D

cement. LR dolomite is present as breccia clasts in mm to cm-scale breccia in one onshore core (15c). LR fabric is distributed most extensively in the LGCP core, including the upper part of the lower peritidal facies assemblage and most of the upper subtidal facies assemblage (Fig. 7). In the Mingan Islands outcrops, the highest percentage (<90%) of LR fabric is observed in the easternmost part of the Sainte Genevieve Member, where it replaces grainy facies and thrombolites. It is also observed as a very minor part (<1%) of the upper subtidal strata of the Grand Île Member in the westernmost outcrop section (Fig. 16). Although uncommon, LR dolomite is present in oolitic dolograinstone in the Norks 86-4 core. In this sample, non-ferroan dolomite perfectly mimics the nonplanar boundaries of early marine calcite cements (Fig. 15d). The cathodoluminescence response of non-planar LR dolomites is dull brick red luminescent to non-luminescent.

Late dolomite cement (LDC) fills and/or overgrows edges of voids and fractures from the sub-micron scale to the cm scale. It is a ubiquitous cement, but unlike late calcite cement, described below, it is rarely the fill in cm-scale voids. LDC dolomite is mainly of ferroan composition. In very fine to medium ER dolomite fabrics, ferroan dolomite fills intercrystalline space, intra-crystalline dissolution voids and submicron-scale fractures along cleavage faces. In submicron-scale sites, the dolomite is usually ferroan and aphanitic overprinting almost all early replacement dolomites in outcrop and core (Figs. 5-9). LDC ferroan dolomite cement with parallel extinction (i.e., planar cleavages) fills larger vugs and fractures as well (Figs.17a, 17b). In vugs and fractures that are incompletely filled, non-ferroan dolomite cement may be the first cement overgrowth on earlier dolomite phase exposed at the void or fracture edge, but ferroan dolomite rims the

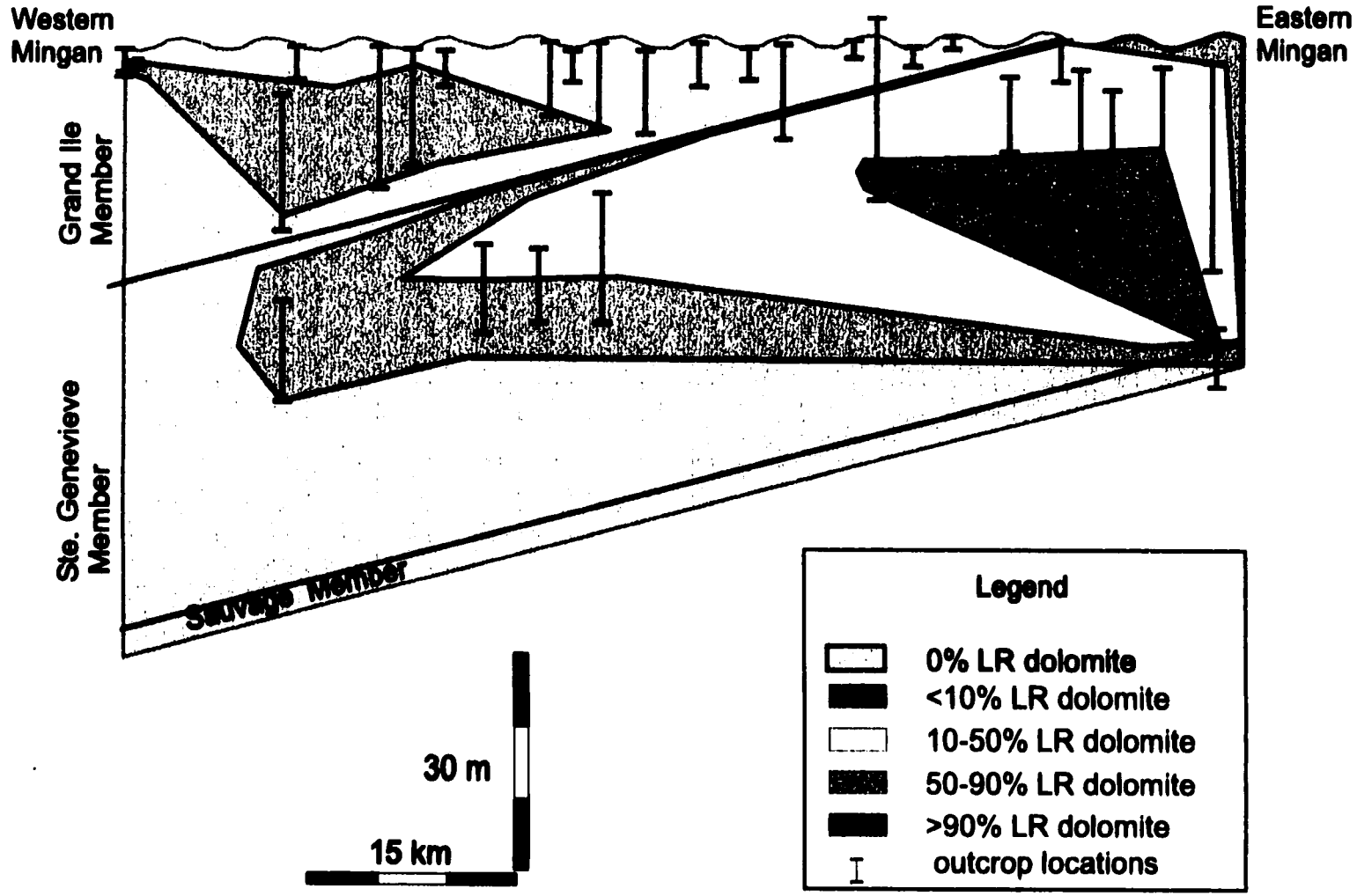

Figure 16. Late replacement dolomite (LR) abundance in the Romaine Formation of the Mingan Islands.

Figure 17

Photomicrographs of LDC, late dolomite cement fabrics

A. Thin section photomicrograph (plane polarized light) of LDC dolomite cement showing the cement filling submicron voids in ER2, planar-s dolomite and 350μm long fracture. Note non-ferroan, euhedral cement overgrowths with ferroan rims on planar-s crystals close to void. Scale bar is 250 μm. Sample source is LGCP core at 5452 ft. depth (1662.2 m).

B. Thin section photomicrograph (plane polarized light) of LDC dolomite cement showing the cement filling submicron voids in LR, nonplanar replacement dolomite and micron-scale fracture. Scale bar is 150 μm. Sample source is LGPL core at 3039 ft. depth (926.5 m).

C. Thin section photomicrograph (plane polarized light) of non-ferroan, saddle dolomite cement showing the cement filling dissolution vug in ER1 dolomicrite. Note sphalerite in narrow fracture at lower center of image. Scale bar is 100 μm. Sample source is NACP core at 5359 ft. depth (1633.8 m).

D. Thin section photomicrograph as C, above (cross-polarized light) showing undulose extinction.

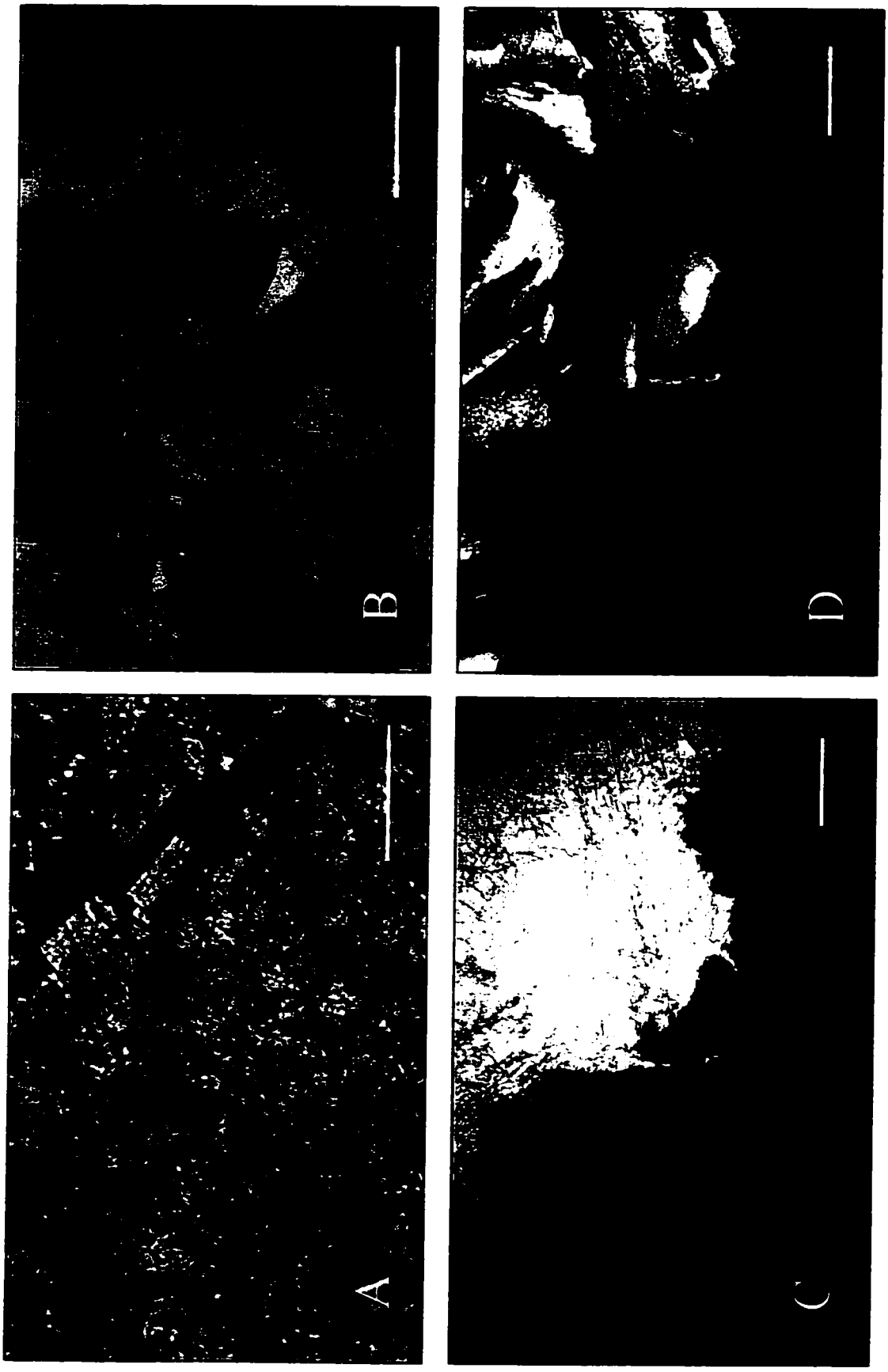
A
B
C
D

non-ferroan phase (Figs. 17a), and, in incompletely filled voids and fractures, the dolomite cement overgrowing earlier phases of dolomite on the edges of the void, commonly has euhedral boundaries in the void space (Figs. 17a).

LDC dolomite cements with curved boundaries and cleavages (saddle dolomite) show undulose extinction (Figs. 17c, 17d, 18a, 18b) can be either non-ferroan or ferroan in composition (Fig. 13d) and their size range varies with the size of the void they fill. The non-ferroan phase is frequently rimmed with ferroan cement (Fig. 18b). LDC dolomite cement with undulose extinction is most common in the eastern portion of the outcrop belt and the NACP and LGCP wells (Figs. 6 and 7). The non-ferroan phase is associated with sphalerite (Figs. 17c, 17d). The cathodoluminescence response of LDC dolomite cements is dull brick red luminescent to non-luminescent.

Calcite fabrics

Three types of calcite fabrics are present in the study area 1) recrystallized depositional fabrics (Figs 11d and 12 a-d), 2) calcitized dolomite (Fig. 18c) and 3) late calcite void and fracture filling cements (Fig. 18c). Recrystallized depositional fabrics are the dominant carbonate fabric in the upper subtidal intervals of the LGPL and NACP drill cores and in the lower subtidal intervals of the LGPL and LGCP drill cores. Dolomitic limestone occurs in the lower subtidal intervals of the NACP drill core (Fig. 6). With the exception of some articulate brachiopods (Fig. 18d), resistant to diagenesis because they are composed of low magnesium calcite (Veizer *et. al*, 1999), primary, depositional calcite is not observed in the thin sections from Anticosti Island cores. A single thin section from the upper subtidal section of the LGPL core shows alternating yellow and orange cathodoluminescent zones. This is interpreted to be early pore-filling calcite (Chi and

Figure 18

Photomicrographs of LDC, late dolomite cement fabrics and calcite fabrics

A. Thin section photomicrograph (cross polarized light) of ferroan, saddle, LDC dolomite cement as a drusy cement in a dissolution void above silica cemented geopetal crystal showing undulose extinction. Scale bar is 500 μm. Sample source is LGCP core at 5452 ft. depth (1662.2 m).

B. Thin section photomicrograph (plane polarized light) of saddle LDC dolomite cement showing non-ferroan core and ferroan rim. Note dissolution of saddle dolomite cements at the edge of the void. Scale bar is 100 μm. Sample source is a outcrop of the St. Geneviève Member in the western Mingan Islands.

C. Thin section photomicrograph (plane polarized light) of calcite brachiopod fragment in showing persistence of early calcite. Note silica cement replacement near center of brachiopod fragment. Note recrystallized trilobite fragements and partially dolomitized matrix. Scale bar is 700 μm. Sample source is LGPL core at 4982 ft. depth (1518.9 m)..

D. Thin section photomicrograph (plane polarized light) of calcitized rhombs overgrowing ER1 dolomicrite. Note preservation of originatal zoning, bitumen, and calcite-filled dissolution voids. Scale bar is 700 μm. Sample source is LGCP core at 3027 ft. depth (922.9 m).

A
B
C
D

Lavoie, 2001). Calcitization or dedolomitization of dolomite occurs most extensively in the LGCP core. It is common in the LGPL core but rare in the NACP cores. Dedolomite occurs as partial or complete calcite replacement of euhedral dolomite rhombs (Fig. 18d). Calcite most commonly replaces the formerly inclusion-rich cores of dolomite rhombs. In the LGCP core, intervals of completely calcitized rhombs occur in association with chlorite in close proximity to LR-rich intervals (Fig. 7). Late calcite void and fracture fills, distinguished on the basis of crosscutting relations, are common to abundant in dolomitized intervals of cores and outcrops (Figs. 5-9). They range from non-ferroan to ferroan cements. They filled cm-scale voids. They occlude porosity in planar-e dolomite fabrics as poikilotopic (up to cm-scale) crystals. Late calcite cements are ubiquitous in the Mingan outcrops and cores (Figs. 7 and 8). They are abundant in NACP and LGCP cores (Figs. 6 and 7), but are less abundant in the LGPL core (Fig. 5).

Other Minerals

Very small amounts of evaporite minerals or their pseudomorphs are observed in the LGPL and NACP cores and thin section suite. Anhydrite beds are present in peritidal intervals (Fig. 10b). Late localized anhydrite nodules and cements, gypsum and barite occur in the LGPL and NACP cores (Figs. 5 and 6; Fig. 19a). 14a). Calcite pseudomorphs of gypsum are present in the NACP core (Fig. 6, Fig. 19b). Silica pseudomorphs of anhydrite occur in thin sections from supratidal facies in the Mingan Islands outcrops.

The MVT minerals sphalerite and barite are present in small amounts in the three Anticosti cores as void and fracture fill and as geopetal deposits in voids (Figs. 5-7, Fig. 19c). Sphalerite is also present in the easternmost sections of the Mingan Islands outcrops

Figure 19

Photomicrographs of evaporites, sphalerite and pyrite

A. Thin section photomicrograph (cross polarized light) of evaporite nodule, showing anhydrite, gypsum and barite in ER1 dolomicrite. Scale bar is 1000 μm. Sample source is LGPL core at 4567 ft. depth (1392.4 m).

B. Thin section photomicrograph (plane polarized light) showing calcite psuedomorphs after gypsum in lime micrite. Scale bar is 40 μm. Sample source is LGPL core at 4528 ft. depth (1380.5 m).

C. Thin section photomicrograph (plane polarized light) of MVT mineralization showing sphalerite in a void filled with late calcite cement. Scale bar is 150 μm. Sample source is NACP core at 5704 ft. depth (1739 m).

D. Thin section photomicrograph (plane polarized light) of MVT mineralization showing euhedral pyrite near dissolution void filled with late calcite cement. Note planar-s ER2 dolomite at the right side of the image. Scale bar is 300 μm. Sample source is NACP core at 5440 ft. depth (1658.5 m).

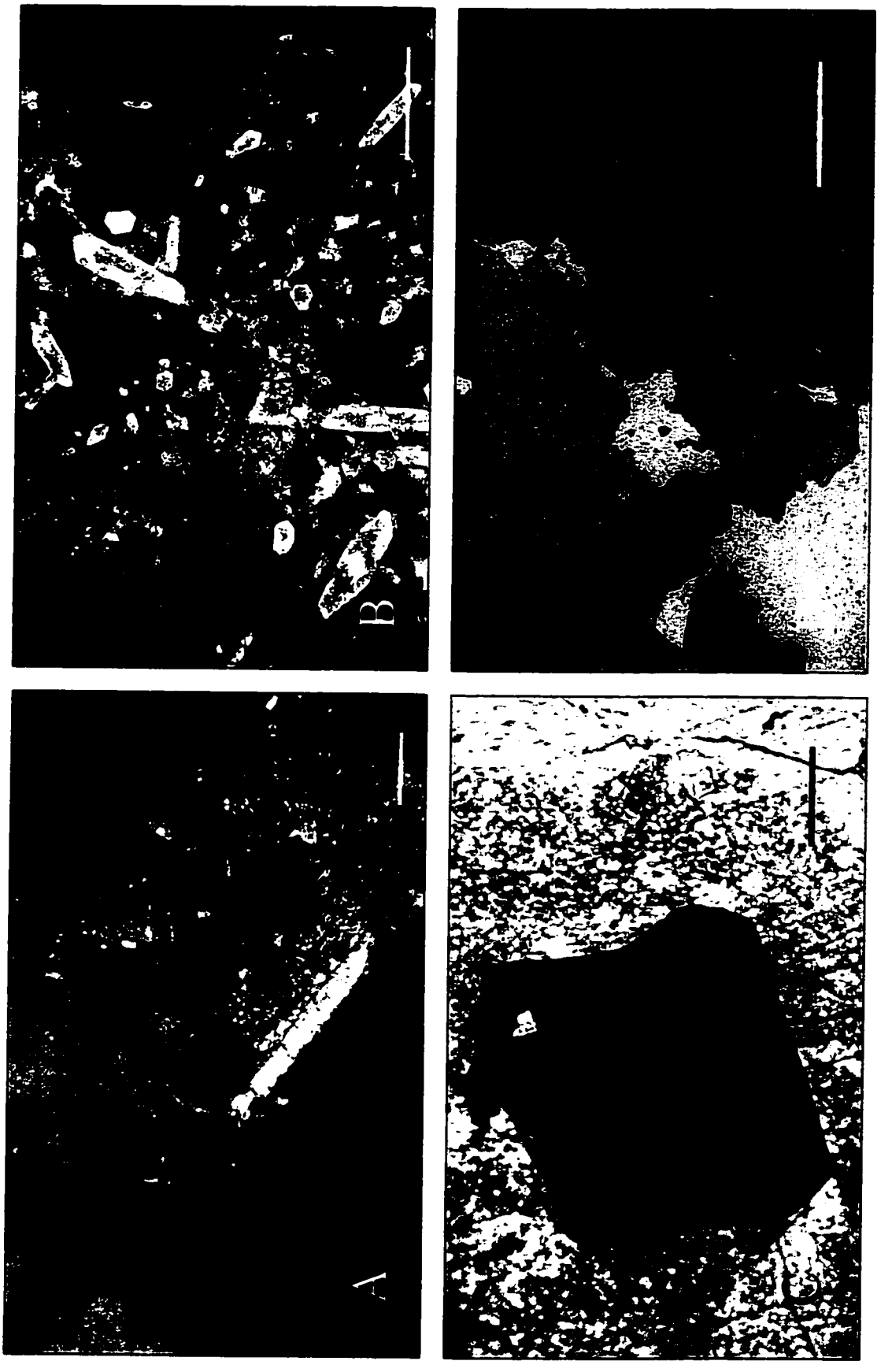
B
A

(Desrochers, pers. com.). Coarse euhedral pyrite is observed in the NACP core (Fig. 19d). It is common in brecciated intervals in the LGCP core and also occurs as massive cements in fractures in LGCP. Early frambiodal pyrite is abundant in both peritidal and subtidal facies. Drillers noted, "brown oil bleeding from core" in Anticosti Island core NACP. Bitumen, and kerogens are present throughout the cores and thin sections. A strong odour of volatiles is noticeable when cutting thin sections and samples.

Cm-scale chert nodules are common in outcrop thin sections and onshore cores. In subsurface cores, mm-scale silica cements are abundant. Some detrital quartz is typically present in peritidal intervals, but it also occurs in subtidal intervals throughout the study area. Quartz also occurs as scattered silt grains in bands of insolubles in shaly partings and solution seams. Late, authigenic, euhedral quartz also occurs associated with euhedral pyrite, sphalerite and with saddle dolomite cement. Late silica cement also occurs as a cement in geopetal crystal debris (Fig. 18a). Rare authigenic feldspar (microcline) is observed in peritidal shaly partings or solution seams. Authigenic muscovite is observed in solution seams and in matrix in both dolomite and limestone facies in the form of highly birefringent "whiskers" or fibres. It is often associated with silica cements and authigenic feldspar. Chlorite is observed in the LGCP core filling allochem molds and in solution seams associated with dedolomite intervals in the lower part of the lower subtidal interval of the LGCP drill core (Fig. 7).

Paragenetic Sequence

Table 3 presents a simplified paragenetic sequence of diagenetic events in early marine, near surface, precompaction burial and deep, syn-compaction burial environments.

Table 3. Simplifed paragenetic sequence

Diagenetic events	Early Marine	Near surface burial	Burial
	Time >	>	>
Deposition and early calcite cements			
Syndepositional to early dolomite (ER1)			
Silica cement			
Early dolomitization (ER2)			
Compaction			
Replacement of porous limestone (LR)			
Dissolution			
Brecciation			
Late dolomite cements (LDC)			
MVT mineralization			
Late silica cement			
Late dolomite cements (LDC)			
Dissolution			
Late calcite cement			
Dissolution			

Stable Isotopes

The $\delta^{13}C$ and $\delta^{18}O$ values of early and late replacement dolomites, dolomite cements, and early and late calcites in the Romaine formation are listed in Table 4. The high, low and average values are shown in Table 5. Early replacement dolomite (ER1 and ER2) has $\delta^{18}O_{PDB}$ values ranging from -10.79 to –4.43‰ (mean = -6.21‰, n = 19) and $\delta^{13}C_{PDB}$ values ranging from –4.91 to –0.29‰ (mean = -2.56‰, n = 19). Late replacement dolomite $\delta^{18}O_{PDB}$ values range from –8.49 to –4.50‰ (mean = -6.52‰, n = 12) and $\delta^{13}C_{PDB}$ values range from –4.10 to –0.31‰ (mean = -1.32‰, n = 12). Comparing ER and LR dolomite stable isotope values, the range of $\delta^{18}O_{PDB}$ values in ER dolmite is wider than for late LR dolomite, but the mean for ER dolomite is similar to that for LR dolomite. For $\delta^{13}C_{PDB}$ values, ER and LR dolomite are very similar in range, but the ER dolomite mean is more negative than the mean for LR dolomite. Late dolomite void and fracture filling cement (LDC) have $\delta^{18}O_{PDB}$ values ranging from –13.79 to –4.43‰ (mean = -8.07‰, n = 7) and $\delta^{13}C_{PDB}$ values ranging from –4.99 to –0.20‰ (mean = -2.73‰, n = 7). Compared to early and late replacement dolomites, LDC stable isotope mean values are more negative. They have the widest range of $\delta^{18}O_{PDB}$ values and the most negative mean value for $\delta^{18}O$; however, the mean $\delta^{13}C_{PDB}$ value is similar to the mean for ER dolomite.

Early calcite has $\delta^{18}O_{PDB}$ values ranging from –8.34 to –6.21‰ (mean = -7.23‰, n = 4) and $\delta^{13}C_{PDB}$ values ranging from –4.22 to –1.76‰ (mean = -2.79‰, n = 4). Late calcite cements have $\delta^{18}O_{PDB}$ values ranging from –14.81 to –5.32‰ (mean = -8.53‰, n = 13) and $\delta^{13}C_{PDB}$ values ranging from –11.60 to –0.08‰ (mean = -3.12‰, n = 13). Early

Table 4. Romaine Formation carbon and oxygen isotope data

Location	Thin Section Number	Lithology	$\delta^{18}O_{PDB}$ ‰	$\delta^{13}C_{PDB}$ ‰
Norks 86-2	13A	Ferroan dolomite cement	-6.59	-0.90
Norks 86-2	13B	Nonplanar replacement dolomite	-6.26	-0.91
Norks 86-2	13C	Planar replacement dolomite	-10.91	-1.25
Norks 86-3	18a	Late calcite cement	-8.95	-0.08
Norks 86-3	18A	Ferroan dolomite cement	-7.20	-0.94
Norks 86-3	18B	Nonplanar replacement dolomite	-6.18	-0.80
Norks 86-3	18C	Nonplanar replacement dolomite	-6.80	-0.95
Norks 86-4	55	Late calcite cement	-10.20	-2.60
Norks 86-4	77	Nonplanar replacement dolomite	-6.99	-1.23
Norks 86-5	15	Late calcite cement	-12.17	-2.08
LGCP	27a	Planar replacement dolomite	-5.26	-1.35
LGCP	27b	Nonplanar replacement dolomite	-4.50	-1.07
LGCP	26	Nonplanar replacement dolomite	-5.93	-0.31
LGCP	25	Ferroan dolomite cement	-5.84	-0.20
LGCP	24	Nonplanar replacement dolomite	-5.91	-0.41
LGCP	21-2	Planar replacement dolomite & ferroan calcite	-6.13	-1.11
LGCP	18	Late ferroan calcite cement	-8.04	-3.68
LGCP	16a	Planar replacement dolomite	-7.40	-1.36
LGCP	16b	Nonplanar replacement dolomite	-6.22	-0.97
LGCP	14	Planar replacement dolomite	-5.96	-0.59
LGCP	9-4	Late calcite cement	-5.32	-1.94
LGCP	8	Planar and nonplanar replacement dolomite	-8.11	-3.15
LGCP	1	Nonplanar replacement dolomite	-7.02	-2.82
NACP	25	Early Calcite	-6.21	-1.76
NACP	23	Early Calcite	-6.48	-4.22
NACP	21	Planar replacement dolomite	-5.60	-2.02
NACP	19	Ferroan dolomite cement	-4.43	-3.87
NACP	17	Planar replacement dolomite	-4.56	-4.57
NACP	15a	Non-ferroan dolomite cement	-8.41	-4.99
NACP	15b	Planar replacement dolomite	-4.43	-3.17

Table 4. Romaine Formation carbon and oxygen isotope data, continued.

Location	Thin Section Number	Lithology	$\delta^{18}O_{PDB}$ ‰	$\delta^{13}C_{PDB}$ ‰
NACP	14	Late ferroan calcite cement	-9.30	-3.96
NACP	13A	Planar replacement dolomite	-4.94	-2.64
NACP	13B	Planar replacement dolomite	-5.36	-2.86
NACP	10	Late calcite cement	-7.36	-11.60
NACP	9	Planar replacement dolomite	-4.38	-4.90
NACP	7	Planar replacement dolomite	-5.67	-3.26
NACP	6	Nonplanar replacement dolomite	-5.59	-0.58
NACP	5	Late calcite cement	-10.46	-2.86
NACP	4	Planar & nonplanar replacement dolomite	-7.48	-2.14
NACP	3	Planar replacement dolomite	-5.51	-0.29
NACP	2	Late calcite cement	-6.78	-2.35
NACP	1	Planar replacement dolomite	-5.60	-0.43
LGPL	45	Late calcite cement	-6.35	-3.10
LGPL	45a	Early calcite	-7.02	-2.53
LGPL	45b	Nonplanar replacement dolomite	-7.86	-2.41
LGPL	42	Late calcite cement	-6.22	-2.68
LGPL	40	Late calcite cement	-5.93	-1.66
LGPL	37	Ferroan dolomite cement	-10.22	-3.46
LGPL	31	Planar replacement dolomite	-5.68	-2.89
LGPL	25	Planar replacement dolomite	-8.49	-2.40
LGPL	22	Late calcite cement	-8.66	-3.57
LGPL	18	Planar replacement dolomite	-7.59	-4.04
LGPL	17	Late calcite cement	-14.81	-2.76
LGPL	16	Late calcite cement	-7.64	-3.32
LGPL	12	Early calcite	-8.34	-2.28
LGPL	6	Ferroan dolomite cement	-13.78	-4.75
LGPL	6a	Nonplanar replacement dolomite	-8.49	-4.10
LGPL	3	Planar replacement dolomite	-7.20	-3.71
LGPL	1	Planar replacement dolomite	-10.79	-4.91

Table 5: Values of $\delta^{18}O_{PDB}$ and $\delta^{13}C_{PDB}$ stable isotope according to mineral type.

Sample source (# samples)	Stable Isotope	Low value (‰)	High value (‰)	Average value (‰)
ER1, 2 dolomite (19)	$\delta^{18}O_{PDB}$	-10.79	-4.43	-6.21
	$\delta^{13}C_{PDB}$	-4.91	-0.29	-2.56
LR dolomite (12)	$\delta^{18}O_{PDB}$	-8.49	-4.50	-6.52
	$\delta^{13}C_{PDB}$	-4.10	-0.31	-1.32
LDC dolomite (7)	$\delta^{18}O_{PDB}$	-13.79	-4.43	-8.07
	$\delta^{13}C_{PDB}$	-4.99	-0.20	-2.73
Early calcite (4)	$\delta^{18}O_{PDB}$	-8.34	-6.21	-7.23
	$\delta^{13}C_{PDB}$	-4.22	-1.76	-2.79
Late Calcite (13)	$\delta^{18}O_{PDB}$	-14.81	-5.32	-8.53
	$\delta^{13}C_{PDB}$	-11.60	-0.08	-3.12

calcite has the narrowest range of $\delta^{18}O$ and $\delta^{13}C$ values. The mean value for $\delta^{18}O$ lies between the means for LR and LDC. The mean $\delta^{13}C$ for early calcite is similar to the means for ER and LDC dolomites. Late calcite cements show the largest range of stable isotope values for both $\delta^{18}O$ and $\delta^{13}C$. The mean values for both $\delta^{18}O$ and $\delta^{13}C$ are the most negative of all carbonates tested.

A cross plot of $\delta^{13}C$ vs. $\delta^{18}O$ values is shown in Figure 20. The early calcite field (solid gray outline) is the narrowest in range. The field of early replacement dolomite (ER) (bold black outline) has a relatively wide range of both $\delta^{18}O$ and $\delta^{13}C$ values; the range of $\delta^{13}C$ values is similar to that of late dolomite cements with which the ER dolomites are intimately intermixed as noted above. Late replacement dolomite (LR) (black outline) is relatively narrow in range for both stable isotope values. Values for late dolomite cements (LDC) fall into two separate groups ((hatched). One group has relatively positive $\delta^{13}C$ values and a relatively narrow range of $\delta^{18}O$ values; the other group has negative $\delta^{13}C$ values with a wide range of $\delta^{18}O$ values. Late calcite cements, except for one extremely negative $\delta^{13}C$ value (see arrow) have a narrow range of $\delta^{13}C$ values and a wide range of $\delta^{18}O$ values, similar to the lower group of LDC.

DISCUSSION

Facies Assemblages

Lateral and vertical distribution of Romaine lithofacies, which recorded the depositional history of the western Anticosti sedimentary Basin, is illustrated in Figure 21.

Figure 20. Crossplot of $\delta^{13}C_{PDB}$ and $\delta^{18}O_{PDB}$ (per mil) for carbonates in the Romaine Formation, Western Anticosti Basin

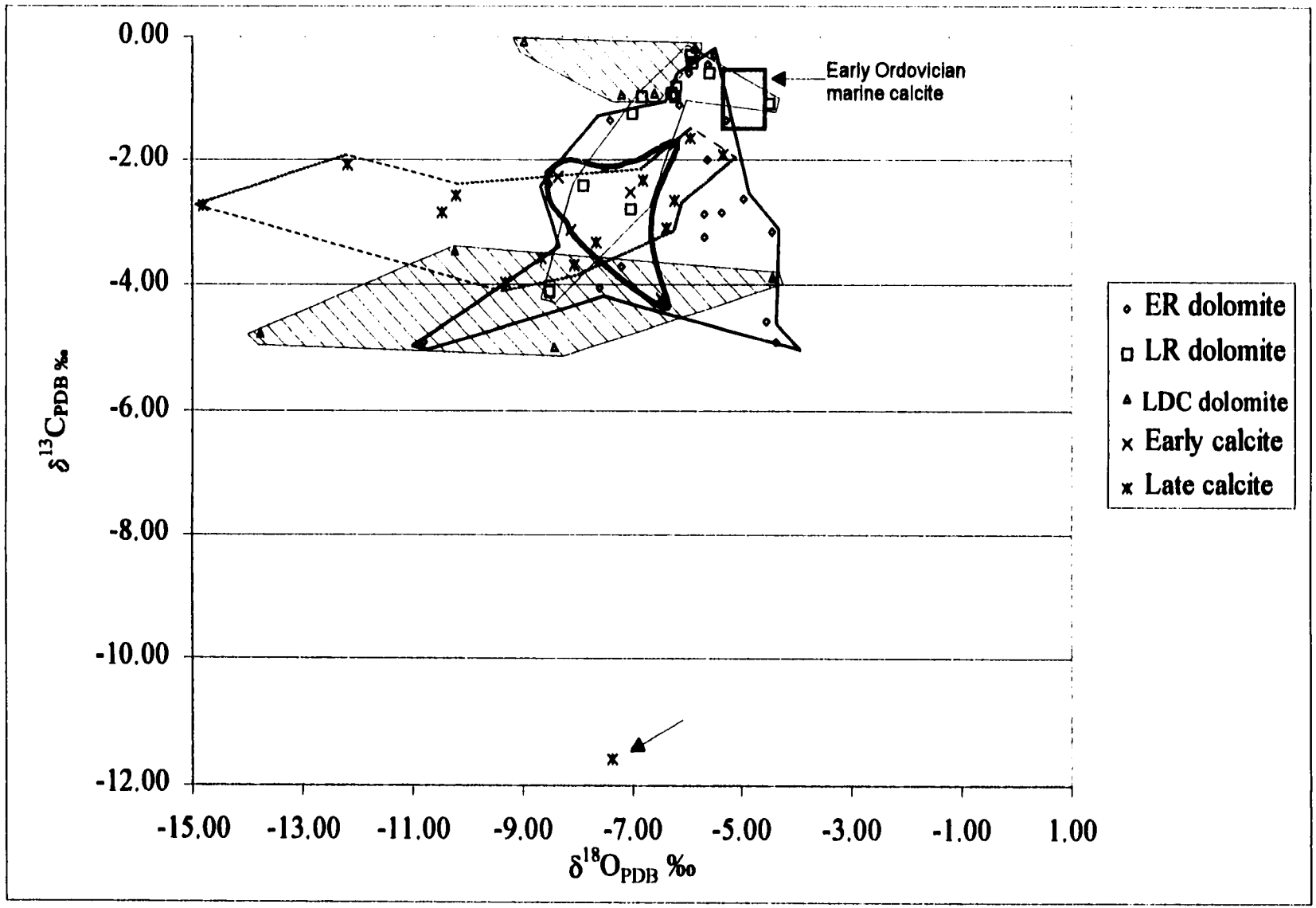

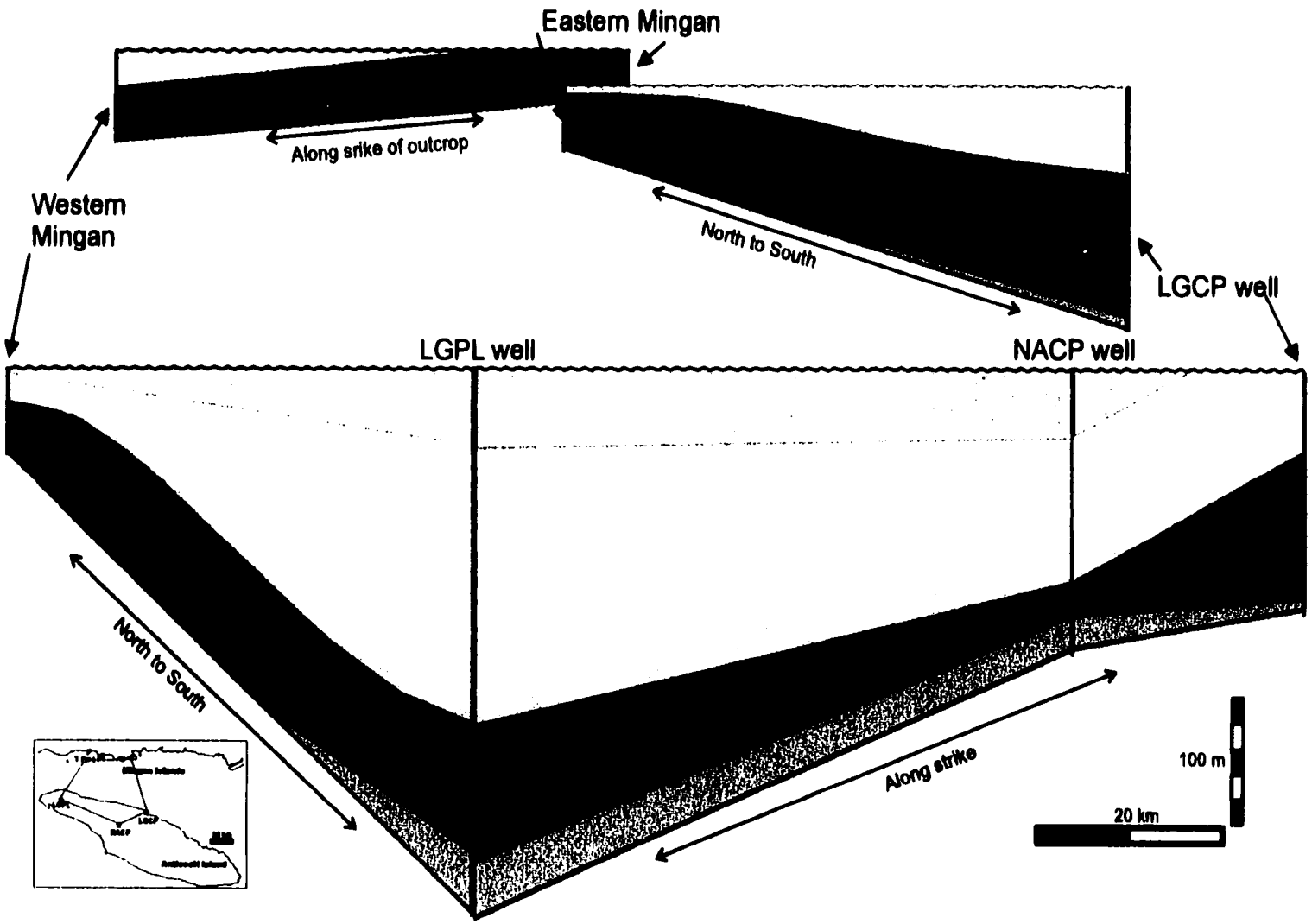

Figure 21. Distribution of lithofacies of the Romaine Formation in the western Anticosti sedimentary Basin. For Legend, see Fig. 4.

This figure represents the western Anticosti Basin in a fence diagram of four panels, two along-strike panels and two north-south panels, which are roughly perpendicular to strike. In the Mingan islands the basal transgressive siliciclastic Sauvage Member blankets the Precambrian basement and is overlain by 1) a subtidal facies assemblage, the St. Geneviève Member, 2) a peritidal facies assemblage, the Grand Île Member, and 3) in the western Mingan only, a second assemblage of subtidal facies, which was not designated a separate unit (Desrochers, 1985, 1988). In the Anticosti Island cores, a discontinuous, thin basal, siliciclastic transgressive lag overlays the Precambrian basement. Above the transgressive lag are four facies assemblages as follows: 1) a lower peritidal facies assemblage, 2) a lower subtidal facies assemblage, facies-equivalent to the St. Geneviève Member, 3) an upper peritidal facies assemblage, facies-equivalent to the Grand Île Member, and 4) in the LGPL and NACP cores, an upper subtidal facies assemblage, similar to the 3 facies assemblage in the western Mingan. The upper subtidal unit is truncated by the Romaine/St. George unconformity.

The distribution of facies assemblages suggests that the basin was filled diachronously from mid- to inner shelf, in response to the most extensive flooding of the platform towards the end of the Early Ordovician time (Pratt and James, 1986; Knight, 1987; Lavoie, 1994). The lower peritidal facies assemblage overlying the basal transgressive lag in the Anticosti cores differs in relative thickness, probably indicating differences in topography on the Precambrian unconformity (Fig. 21). The lower peritidal facies assemblage includes small amounts of evaporites in LGPL (Fig. 4) and NACP (Fig. 5), suggesting that the rate of relative sea level rise did not keep up with sedimentation rate (Walker and James, 1992). The lower peritidal facies assemblage is not present in the

Mingan outcrop belt. The transgressive Sauvage Member is overlain by the lower subtidal facies assemblage/St. Geneviève Member which is present in both the Mingan and Anticosti Island subsurface. It is anomalously thin in the NACP core (Fig. 5). This may be because the NACP penetrates an intertidal island that developed during the initial flooding and deposition of peritidal facies, persisted through the early part of the deposition of subtidal facies on other parts of the mid shelf, and; thus, received less subtidal sedimentation than other areas of the shelf. This interpretation is supported by the presence of relatively frequent ooids in the lower peritidal interval of the NACP core, an indication of high-energy depositional environment. The subtidal interval has relatively high volumes of LR dolomite in the NACP core, and, as mentioned above, inclusions in the LR dolomite outline elements of porous precursor packstone and grainstone textures. Pratt and James (1986) proposed a tidal flat island model for carbonate sediments of the St. Lawrence Platform as recorded in the St. George Group of western Newfoundland. Over the study area, the base of the lower subtidal assemblage/ St. Geneviève Member is dominated by tempestites. These are overlain by intensely bioturbated mudstones, bioclastic and intraclastic wackestones and packstones. In the Mingan outcrops and cores, thrombolite reefs and inter-reef facies dominate the upper part of the St. Geneviève Member indicating overall shallowing of the environment of deposition. In the Anticosti cores, inter-reef facies (Fig.12b) in the upper part of the lower subtidal facies assemblage are evidence for a shallowing upward through the interval. The upper peritidal facies assemblage/Grand Île Member overlies the lower subtidal facies assemblage/St. Geneviève Member in the study area. The cyclic nature of the peritidal facies assemblage is apparent in the Mingan Islands, where outcrops give three dimensional, megascopic views of facies

changes (Desrochers, 1985, 1988). In the Anticosti cores facies changes are commonly obscure. However, there is an overall shallowing up; evaporites occur in the upper portion of the interval in the LGPL and NACP cores (Figs. 4 and 5), indicating general shallowing through the interval. An upper subtidal facies assemblage is present in the western part of the basin in both cores and outcrop, but is not present in the east. In the Mingan Islands, beds are progressively truncated from west to east by the regional unconformity (Desrochers, 1985, 1988). The upper subtidal facies assemblage differs from the lower subtidal unit. The upper subtidal facies assemblage is muddier, no thrombolite is observed, the fauna, dominated by gastropods, is somewhat less diverse than in the lower subtidal unit and pseudomorphs of evaporites occur in the limestone matrix (Fig. 19b). These are indications of a lower energy regime and a more restricted basin than in the lower subtidal facies assemblage. This unit records a relative rise in sea level prior to or in conjunction with the Taconic Orogeny, which is not recorded or not preserved in other parts of the platform. This suggest that tectonic loading of the platform at the onset of the Taconic orogeny resulted in an overall local relative sea level rise. The peripheral bulge restricted circulation in the basin as it migrated westward (James *et al.*, 1989).

Sequence stratigraphic framework

Sequence stratigraphy uses unconformities and flooding surfaces to determine genetically related lithofacies; this is the basis for analysis of basin evolution in terms of tectonic processes and relative sea level changes (Walker and James, 1992). The sequence stratigraphic framework of the Romaine Formation is shown in Figure 22. In the western Anticosti Basin, two large-scale, third order sequences are recorded (Desrochers, 1985;

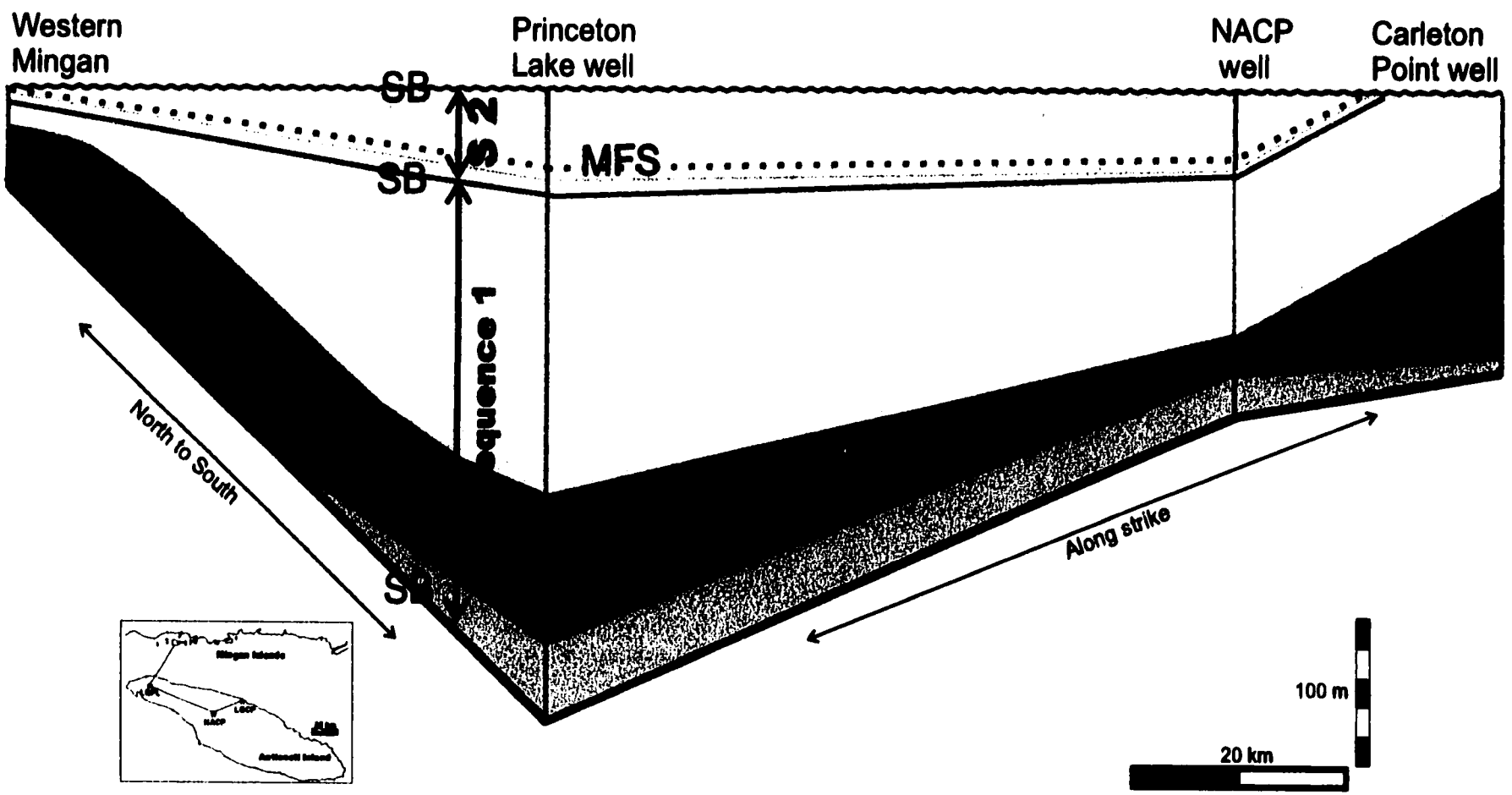

Figure 22. Sequence stratigraphic framework of the Romaine Formation of the western Anticosti sedimentary Basin. For legend, see Fig. 4.

James *et al.*, 1989). The sequence boundary underlying the first sequence is the Precambrian unconformity (Knight *et al.*, 1991). The initial flooding of this part of the St. Lawrence Platform is marked by the thin basal transgressive lag in the mid shelf and by siliciclastic sand in the inner shelf outcrop belt. During slow rate of sea level rise, peritidal facies developed in the mid shelf. When the rate of sea level rise increased, a lower subtidal facies developed in the inner and mid shelf. There was no clear maximum flooding surface in Anticosti cores, instead there was a zone of transition between peritidal facies and deeper water facies. The line for maximum flood is interpreted above the calcarenite tempestites in the LGPL core, at the highest observed bored hardground in LGCP. In NACP no single surface is designated maximum flooding surface. With progradation during highstand, facies belts moved basinward, stacking shallower facies over deeper facies. Thrombolite reef complexes developed on the inner shelf (Desrochers, 1988) and individual mounds or not reef complexes developed in mid shelf; there is not enough well control to tell how extensive mound development was in the mid shelf. An upper assemblage of cyclic peritidal facies developed above the subtidal facies assemblage as progradation of the shoreline continued through the highstand. A non-erosive sequence boundary between the first and second large-scale sequence is placed above the uppermost evaporite occurrence, before the second transgression. Conodont biostratigraphic work supports the case for a paraconformable, non-erosive boundary (Nowlan, 1984), which means that sea level did not fall below the shelf margin. The second large-scale sequence is marked by a deeper water facies overlying supratidal evaporitic facies. In the western part of the basin, an upper subtidal facies assemblage was deposited over upper peritidal facies. A maximum flooding zone is indicated rather than a distinct maximum flooding

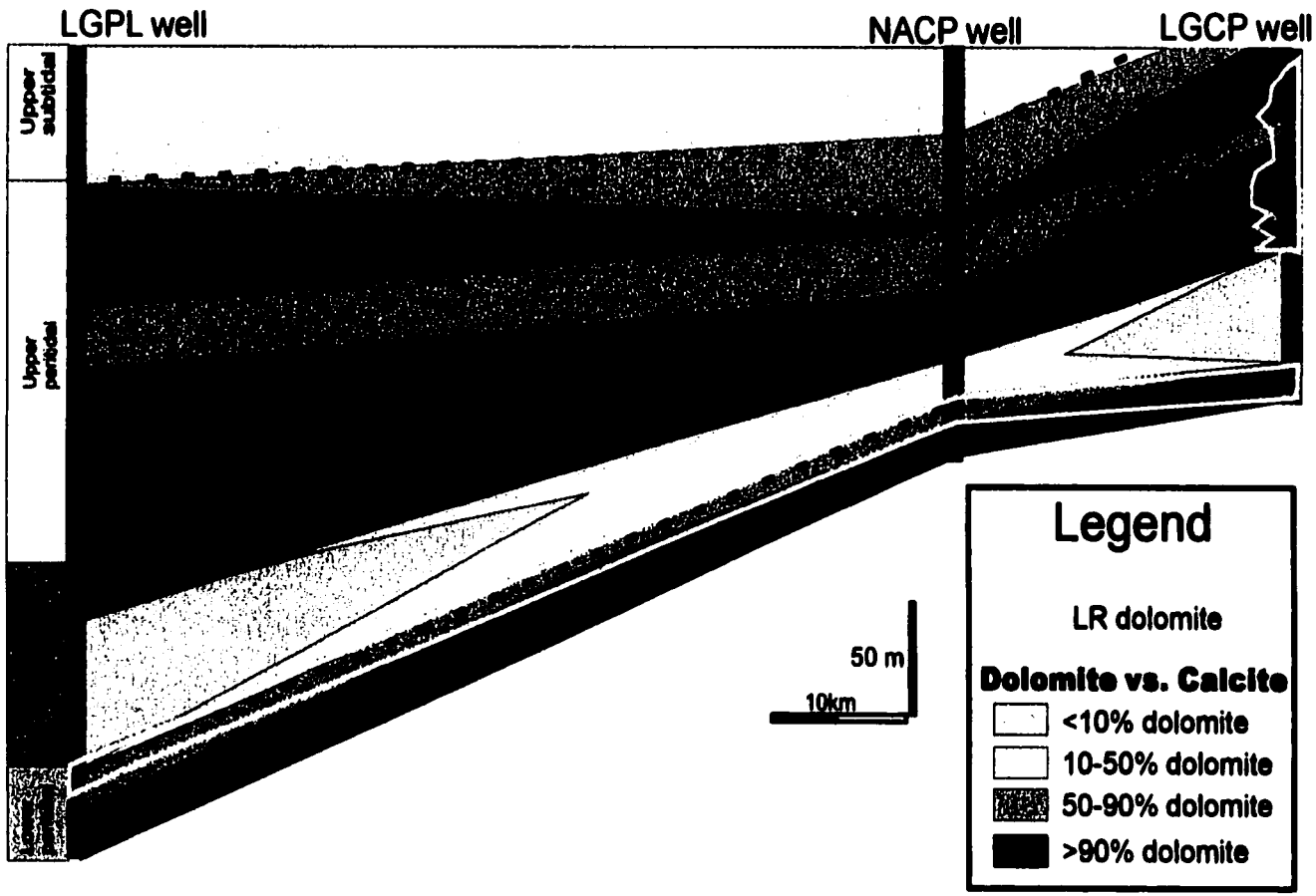

Figure 23. Dolomite abundance in three Anticosti Island cores with the occurrence of LR dolomite.

surface. The regional Romaine/St. George unconformity developed during uplift with the onset of the Taconic orogeny. It is the regional sequence boundary, and the boundary at the Sauk/Tippecanoe cratonic sequence (Desrochers, 1988; Knight *et. al.*, 1991).

The facies assemblages of the mid-shelf LGPL core are correlated with the St. George Group on the basis of lithofacies and sequence stratigraphic surfaces in Figure 3. The basal transgressive lag correlates with the "Pebble Bed" in the St. George Group; the lower peritidal facies assemblage is correlated with the upper Boat Harbour Formation (Brennan-Alpert *et al.*, 2001); the lower subtidal facies assemblage/St. Genevieve Member is correlated with the Catoche Formation, and the upper peritidal facies assemblage/Grand Île Member is correlated with the Aguathuna Formation (Desrochers, 1988). As in the eastern part of the study area, the upper subtidal facies assemblage is absent in the St. George Group; either never deposited or eroded. In western Newfoundland, the mid Whiterockian to Chazyan Table Head Formation overlies the St. George Unconformity (Stenzel and James, 1990). In the western Anticosti Basin, the Mingan Formation overlies the unconformity (Desrochers, 1985).

Dolomite Fabrics

The distribution of dolomite in the Romaine Formation is summarized in two figures. Figure 16 represents the types of dolomite in the pervasively dolomitized Mingan outcrops and cores. Figure 22 represents dolomitization and types of dolomite in the three Anticosti cores. Two trends are shown. Dolomitization decreases basinward and peritidal facies are preferentially dolomitized. The pattern of decreasing dolomitization basinward is similar to the rest of the "Great American Bank" where the inner shelf is pervasively dolomitized and the outer shelf is limestone with little dolomitization (Harris, 1973, as

cited in Blatt, 1992). The mid shelf Anticosti cores reflect their transitional position; peritidal facies are pervasively dolomitized, but subtidal facies are partially dolomitized to non-dolomitized. In the calcitic dolomite (50-90% dolomite) portions of both the lower and upper peritidal facies assemblages in the Anticosti cores, the calcite is late poikilotopic cement, rather than undolomitized limestone elements. Subtidal facies assemblages are pervasively dolomitized in the Mingan Islands and partially dolomitized in the Anticosti cores. With the exception of the LGCP core, skeletal elements and burrows are dolomitized and there are scattered rhombs in lime micrite matrix, which may be concentrated near solution seams. Again, except for the LGCP core, planar ER dolomites are the dominant dolomites in upper and lower peritidal facies assemblages. Planar, ER dolomites are associated with peritidal facies and with the inner shelf environment. Nonplanar, LR dolomites present a different distribution trends. First, LR dolomite is present in all three Anticosti cores associated with the transition from peritidal to subtidal facies. In many thin sections from this transition zone, inclusions in LR dolomite fabrics outline precursor packstones and grainstones. In the LGCP core, nonplanar LR dolomite makes up >50% of dolomite in thin sections from the lower peritidal and lower subtidal facies assemblages. LR dolomite is present in small amounts (<40% in one thin section) in the NACP core, but makes up more than half the dolomite in thin sections in the LGPL core. This suggests that the lower peritidal facies assemblage in the Anticosti cores retained undolomitized limestone clasts until the influx of LR-precipitating fluids, and that late dolomitizing fluids moved laterally through porous zones. A second type of LR dolomitization occurs in thin sections from the upper peritidal facies assemblage of the LGCP core, where LR dolomite makes up more than half the dolomite

in some intervals. In this section, nonplanar LR dolomite is associated with brecciation in the core. In this case, the LR dolomitizing fluids may have been focused along faults. Both lateral movement of late dolomitizing fluids through porous facies and focusing of late dolomitizing fluids along faults are seen in the Upper Knox dolomite (Montanez, 1992, 1997), in the Michigan Basin (Middleton *et al.*, 1993) and in hydrothermal systems in the Western Canadian Sedimentary Basin (Reimer and Teare, 1999; Van Zeeg and Davies, 1999). In the Mingan Islands, nonplanar LR dolomite is present in traces throughout outcrops of the subtidal St. Geneviéve Member the Mingan Islands; however, it occurs in high percentages in only a few thin sections in the eastern Mingan (Fig. 16). Nonplanar, LR dolomite occurs in trace amounts in the western Mingan Grand Île Member. Seismic data and information from exploratory wells east of the study area on Anticosti Island support the interpretation that late dolomitizing fluids moved along along faults and laterally into porous zones (Lynch, 2001). The eastern Mingan and LGCP nonplanar LR dolomites may represent the distal expression of fluids moving along faults from the east.

Dolomite fabrics, defined by size and shape of crystals are controlled by a complex of interrelated factors as follows: depositional textures of precursor limestones, changes of temperature, pressure and fluid chemistry during diagenesis (Sibley and Gregg, 1987; Montañez and Read, 1992; Kupecz, *et. al.*, 1993; Warren, 2000). Of these factors, temperature is usually the most important. Although crystal size depends on the ratio of nucleation rate to growth rate, higher temperatures of dolomitization yield relatively coarser crystals (Sibley and Gregg, 1987). The shape of crystal boundaries is also dependent on temperature. At temperatures approxiamtely 50°-100°C, growth of crystals

occurs by nucleation at active sites followed by orderly growth, yielding crystals with planar euhedral or planar subhedral compromise boundaries. Above 50°-100°C, crystals grow by random addition of atoms to the surface; non-planar, irregular boundaries result. Again, though there are exceptions, dolomite fabrics with planar-e or planar-s boundaries are low temperature dolomites; those with nonplanar boundaries are generally high temperature dolomites (Gregg and Sibley, 1984; Sibley and Gregg, 1987).

Low temperature dolomite has been difficult to study because it has not been synthesized in the laboratory except at temperatures above 50° or 60°C (Hardie, 1987). Recently, however, Vasconcelas, cultured sulfate reducing bacteria (SRB) from a dolomite producing, hypersaline lagoon in water adjusted to match the composition of the lagoon. After a year in a refrigerator at 4°C, dolomite was found to have precipitated on bacterial surfaces (Vasconcelas, et. al., 1995). This suggests barriers to nucleation at low temperatures can be bypassed biotically and that low temperature/low pressure dolomite as formed in evaporitic/sabkha environments (Vasconcelas and McKenzie, 1997; Wright, 1999; Warren, 2000).

ER1 dolomite fabrics, very fine (4-16μm), to finely crystalline (16-62μm) and planar, are interpreted to have formed by synsedimentary precipitation and/or replacement of calcitic and aragonitic sediments in intertidal to supratidal evaporative or sabkha environments. Medium crystalline, subtidal, ER2 dolomite textures are interpreted to be the product of dolomitization in an early burial environment in mixing zone conditions (Desrochers, 1988; Haywick, 1984; James, 1989; Montañez, 1992). Though many questions about the mixing zone model are as yet unsolved, investigations into the role of bacterial involvement in dolomitization are a promising new development (Hardie, 1987;

Lumsden, 2001; Warren, 2000). There are differences in crystal size between inner and mid shelf ER1 dolomite fabrics. In samples from the inner shelf, Mingan outcrops, both ER1 matrix dolomite and allochems (gastropods and a restricted fauna, pellets and ooids) are finely crystalline (Desrochers, 1988). In the middle shelf setting, allochems in peritidal facies may be replaced by fine to medium crystalline dolomite (Sibley and Gregg, 1987). It is accepted that initially very fine grained, ER1 dolomites increase in size in near surface burial and through recrystallization (Kupecz *et al.*, 1993; Warren, 2000). Later fluids modify early-formed dolomites. Directly precipitated dolomite in modern settings is first precipitated onto bacteria bodies (Thompson and Ferris, 1990; Shultze-Lam, *et. al.* 1992, 1996) and appears in SEM micrographs as spherical bodies (Folk, 1993; Wright, 1999; Gournay, 1999; Warren, 2000). As they are buried in the sediment dolomite crystals, both directly precipitated and replacement types, grow in size. Early ordering, isotopic signatures and trace minerals are reset (Kupecz *et al.*, 1993; Vasconcelas and McKenzie, 1997; Warren, 2000). With deeper burial, early dolomite fabrics may be overgrown with later phases of dolomite, dissolved and recrystallized by later fluids (Kupecz, 1993; Warren, 2000). Since inner shelf ER1 dolomite fabrics retain their fine grain size, it is interpreted that processes tending to increase crystal size were cut short in the inner shelf, but persisted in the mid shelf. Alternatively, inner shelf sediments may have been muddier than those of the midshelf; high ratio of nucleation sites to crystal growth rate may have restricted grain size in the inner shelf (Sibley and Greg, 1987).

LR dolomite is interpreted to have precipitated at temperatures above 50-100 °C (Sibley and Gregg, 1987). LR dolomite replaces porous packstone or grainstone; the precursor fabric is outlined in inclusions in the late replacement dolomite. Most LR

dolomite does not bear solution seams or stylolites, but in one instance (Fig. 14b) an LR breccia clast bears a solution seam. The breccia clasts float in a dark siliceous or organic matter-rich matrix with ~10% individual, planar-e dolomite rhombs. A solution seam also cuts the breccia. This indicates that LR dolomite began replacing porous limestone before an early phase of compaction and continued to form as compaction continued. LR dolomite is visually remarkable amongst the dolomites of the Romaine Formation in that it is generally clean and clear of all but the slightest ferroan overprint. It stands out bright and unstained in thin sections, in a field of blue-stained, inclusion-rich, "dirty" dolomites. LDC dolomite cements vary in composition from non-ferroan to ferroan. They vary in shape from crystals with planar boundaries and/or parallel extinction to spear-shaped crystals with curved boundaries and/or undulose extinction. Aphanitic ferroan dolomite fills submicron- to micron scale voids and fractures in earlier phases of dolomite. Where LDC crystals line dissolution voids or fractures, non-ferroan, planar or saddle dolomites have ferroan rims of either planar or nonplanar types. Saddle dolomite precipitates at temperatures above 60°C (Radke and Mathis, 1980; Gregg and Sibley, 1984; Reimer and Teare, 1992; Warren, 2000). Non-ferroan saddle dolomites are interpreted to precipitate after some dissolution of both ER and LR replacement dolomite fabrics (Table 3). Saddle dolomite crystals, sphalerite crystals and coarse euhedral pyrite crystals occupy dissolution voids, often in association with fine crystal debris which is also often cemented with silica (Figs. 24a, 24b, 18a, 19c, 19d). Ferroan saddle or planar LDC dolomite often overgrows non-ferroan saddle or planar phases, but the reverse is never observed. This suggests there were at least two major pulses of warm dolomitizing fluids. The early fluids dissolved/replaced laterally continuous packstones and grainstones with LR dolomite.

Figure 24

Photomicrographs showing late diagenetic events

A. Thin section photomicrograph (plane polarized light) of spearhead-shaped, ferroan saddle LDC cement overgrowing planar ER2 dolomite and non-ferroan LDC cement overgrowths at edge of dissolution void. Last void-fill is late calcite cement. Scale bar is 700 μm. Sample source is Norks core 86-4.

B. Thin section photomicrograph (plane polarized light) showing nonferroan saddle LDC overgrowing nonplanar LR dolomite at dissolution edge, and overgrown by ferroan saddle LDC cement. Scale bar is 200 μm. Sample source is Norks core 86-4.

B
A

iron rich phases infiltrated submicron spaces in ER1 and ER2 dolomite. The second fluid pulse dissolved LR fabrics and ER fabrics, was associated with microbrecciation, silicification, and precipitation of nonferroan saddle dolomite, sphalerite and pyrite, and ferroan overgrowths on earlier phases. Calcite preciptiating fluids followed a dissolution event that corroded earlier phases. A minor ferroan LDC precipitating fluid followed the first calcite cementation event and it was followed by a final calcite precipitating fluid. The fluids that precipitated calcite were high temperature fluids as will be discussed below (Chi and Lavoie, 2001).

Stable Isotopes

Fractionation of naturally occurring isotopes by chemical, physical and biological processes changes distribution patterns in a measurable way and, with corroborating evidence of trace elements, radiogenic isotopes and fluid inclusions, variations in isotope patterns indicate the processes that influenced the distribution patterns (Allan and Wiggins, 1993). It is generally accepted, however, that $\delta^{18}O$ values in early carbonate phases can be reset by influence of later dolomitizing fluids, *i.e.*, dolomite that is petrographically consistent with an early diagenetic orgin (fine to medium crystalline, planar dolomite) may lose the early diagenetic $\delta^{18}O$ signature (Mackenzie, 1981; Kupecz *et. al.*, 1993; Vasconcelas and Mackenzie, 1997; Warren, 2000). Because fractionation of oxygen isotopes is less efficient at higher temperatures, higher temperature phases are expected to have more negative $\delta^{18}O$ values than low temperature phases (Allan and Wiggins, 1993; Gregg, et. al., 2001). Three distribution patterns suggest that earlier $\delta^{18}O$ isotope signatures were influenced by later, high temperature (>60°C) dolomitizing fluids. First, there is considerable overlap of $\delta^{18}O$ values (Fig. 20). Second, the values for early

calcite are more negative (Fig. 20) than values generally accepted in the literature [approximately -5‰ (Lohmann, 1989)]. And third, $\delta^{18}O$ isotope values for Ordovician dolomite are mostly lighter than Ordovician marine calcite $\delta^{18}O$ values instead of the expected 3 to 6‰ heavier values (Tucker and Wright, 1990; Allan and Wiggins, 1993).

Looking at $\delta^{18}O$ values for individual early phases (Fig. 20), Early calcite has the narrowest range of values, between 1 and 3‰ more negative than estimated values for early Ordovician marine calcite (Lohman, 1989). Early replacement dolomite has a very wide range of values, which will be discussed below, but in late replacement dolomite eight out of twelve data points are within 1‰ of the range of values for early marine calcite; the other four samples have slightly lighter (2 to 3‰) $\delta^{18}O$ values than early calcite. The pattern of values for late replacement dolomite suggests that signature of the higher temperature, LR phase has been influenced by the isotope signature of the precursor limestone (Warren, 2000).

Late dolomite cement isotope values fall into two groups. The first has a narrow range of $\delta^{18}O$ values close to the range of values for early calcite, and a range of $\delta^{13}C$ values that overlap or are up to 4‰ more negative than those for early Ordovician marine calcite(Fig. 20). The second group of LDC values has a very wide range of $\delta^{18}O$ values and narrow range of $\delta^{13}C$ values that is more than 2‰ more negative than early Ordovician marine calcite. This supports the petrographic observation that there were at least two phases of cementation by late, high temperature dolomitizing fluids. The $\delta^{18}O$ values of the first LDC group are equal to or slightly more positive than early marine calcite; the $\delta^{13}C$ values are slightly more negative. This is consistent with what is expected in a closed system in which there is low fluid to rock interaction. Intraformational waters

are heated with burial; earlier phases are cannibalized and higher temperature dolomites are precipitated (Montañez, 1992, Warren, 2000). The $\delta^{18}O$ values of the second LDC group range from 8‰ more negative than early Ordovician marine calcite to slightly more positive than early Ordovician marine calcite. The $\delta^{13}C$ values fall into a narrow range from 2 to 4‰ more negative than early Ordovician marine calcite. This pattern suggests the second phase of late dolomite cement was precipitated from warm fluids in an open system in which the fluid to rock ratio was relatively high (Montañez, 1992, Warren, 2000). Reviewing the pattern for late replacement dolomite, most isotope values (eight out twelve) fall within or close to the range outlined for the first, closed-system, phase of late dolomite cement. This suggests that most LR dolomite was precipitated close to the same time as the first phase of late dolomite cement in a closed system from an intraformational burial fluid.

To interpret the very wide range of isotope values for early replacement dolomite (Fig. 20), it should be recalled that this phase is intimately mixed with late ferroan dolomite cement which fills sub-micron voids and fractures. No single-phase ER samples were tested. Thus the range of ER isotope values reflects the range of LDC values. ER $\delta^{18}O$ values are generally more positive than LDC values, reflecting both the signatures of the precursor limestone and the signatures of the low temperature ER dolomite. Values for $\delta^{13}C$ in ER dolomite match the range of values in LDC dolomite. This is not consistent with the conservative nature of $\delta^{13}C$ signatures (Allen and Wiggins, 1993), but may reflect a very high fluid to rock interaction in samples with very negative values.

Hydrothermal and burial origins

Organic matter reflectance studies and recent fluid inclusion work on the Romaine

Formation show temperature ranges of 115°-147°C and 131°-137°C, respectively (Bertrand, 1990; Chi and Lavoie, 2001). These temperatures can account for the presence of nonplanar replacement dolomite (LR) and saddle dolomite (Warren, 2000; Chi and Lavoie, 2001). Burial at depths estimated for the Romaine Formation is sufficient in all three cores (3.3 km - 4 km, and 4.5 km in the Mingan Islands) to result in the estimated temperatures depending on the assumed geothermal gradients (Bertrand, 1990; Warren, 2000; Chi and Lavoie, 2001). However, the proximity of known hydrothermal deposits (*i.e.*,the economic sphalerite deposit at Daniel's Harbour) closer to the edge of the St. Lawrence Platform (Haywick, 1984; Lane, 1990; Kesler, 1996; Cooper *et al.*, 2001; Chi and Lavoie, 2001) and, as Chi and Lavoie (2001) pointed out, similar diagenetic products and style of dolomitization, make the hydrothermal model a strong possible explanation of the latest diagenetic products in the Romaine Formation. Because the peak temperature is reached before the end of precipitation of burial cements in the Anticosti cores, Chi and Lavoie (2001) propose a significant hydrothermal event occurred. Supporting this interpretation is proximity to confirmed hydrothermal deposits in time equivalent units in the outer shelf. Non-ferroan, saddle dolomite and LR fabrics are reported in the district of the Daniel's Harbour Zinc mine (Lane, 1990, Kesler, 1996). South of Daniel's Harbour, these high temperature phases are reported in the partially dolomitized St. George Group as matrix replacement in Pervasive B dolomite (Haywick, 1984) and in Shell Canada wells in the eastern sector of Anticosti Island (Lynch, pers. comm.).

CONCLUSIONS

1. Romaine Formation strata in the western Anticosti Basin consist of inner to midshelf.

Muddy, bioclastic carbonates, which form a lopsided wedge, which is thickest in the midshelf, ranging from 430 m in the LGPL well to 180 m in the LGCP well on the flank of the Beaugé Arch. The wedge is thinnest in the inner shelf ranging from 70 m in the western Mingan outcrop belt to ~30 m in the eastern Mingan outcrop belt.

2. Pervasively dolomitized peritidal and pervasively to partially dolomitized subtidal facies assemblages are stacked in two large scale sequences, the first sequence is capped by a non-erosive sequence boundary indicating that sea level did not fall below the shelf edge. The second sequence is recorded in the western part of the western Anticosti basin but not in the eastern part where it is truncated by the sequence boundary. The first sequence is correlated with the St. George Group.
3. Two major stages of replacement dolomitization are distinguished petrographically on the basis of size and shape of crystals: 1) an early stage of planar, very fine to medium crystalline, low temperature replacement dolomite and 2) a late, non-planar, medium to coarsely crystalline, high temperature (>60°C) replacement dolomite. Two phases of late dolomite cements are distinguished petrographically on the basis of crosscutting relationships.
4. At least two phases of high temperature (>60°C) dolomitization are distinguished on the basis of stable isotope signatures. The earlier phase precipitated nonplanar, late replacement dolomite and non-ferroan and ferroan late dolomite cements in a closed system in which $\delta^{18}O$ and $\delta^{13}C$ signatures reflect the values of precursor limestone. The second phase precipitated non-ferroan and ferroan late dolomite cements with a wide range of $\delta^{18}O$ values and a narrow range of $\delta^{13}C$ values, in a open system from warm fluids.

REFERENCES

Allan, J. R. and Wiggins, W. D. 1993. Dolomite Reservoirs: Geochemical techniques for evaluating origins and distribution. AAPG Continuing Education Course Notes Series, 36, 129p.

Bernstein, L. 1992. A revised lithostratigraphy of the lower-middle Ordovician Beekmantown Group, St. Lawrence Lowlands, Quebec and Ontario, Canadian Journal of Earth Science, 29, 2677-2694.

Bertrand, R. 1987. Maturation thermique et potentiel pétroligène des séries post-Taconiennes du nord est de la Gaspésie et de l'île Anticosti, Canada. Unpublished doctoral thesis, Université de Neuchâtel.

Bertrand, R. 1990. Maturation thermique et histoire de l'enfouissement et de la génération des hydrocarbures du bassin de l'archipel de Mingan et de l'île Anticosti, Canada. Canadian Journal of Earth Science, 27, 731-741.

Blatt, H. 1992. Sedimentary Petrology. W. H. Freeman and Company, New York. 514p.

Bolton, T. E. 1970. Subsurface Ordovician fauna, Anticosti Island, Quebec. GSC Bulletin 187, 31-41

Brennan-Alpert P., Desrochers, A., Lavoie, D., and Chi, G.S. 2001. Basin-wide dolomitization patterns along the Lower Paleozoic Laurentian continental margin, Anticosti Basin, Eastern Québec. Oral presentation to the C.S.P.G. annual technical convention "Rock the Foundation", June 18-21, program with abstracts pp. 023-1-023-2.

Chi, G. and Lavoie, D. 2001. Diagenesis of dolomites in the Romaine Formation, Anticosti Island. Current Research, 2001-D.

Churnet, H. G. and Misra, K. C. 1981. Genetic implications of the trace element distribution pattern in the Upper Knox carbonate rocks, Copper Ridge district, east Tennessee, Sedimentary Geology, 30, 173-194.

Cooper, G. A. 1956. Chazyan and related brachiopods. Smithsonian Miscellaneous Collections; 127, Pt.1, 1024p.

Cooper, M., Weissenberger, J., Knight, I., Hostad, D., Gillespie, D., Williams, H., Burden, E., Porter-Chaudhry, J., Rae, D., and Clark, E. 2001. Basin evolution in western Newfoundland: new insights from hydrocarbon exploration. AAPG Bulletin, 85, 393-418.

Davies, G. R. 2000. Hydrothermal dolomite reservoir facies: global and western Canadian perspectives. Grahman Davies Geological Consultants, Ltd.. 214p.

Demicco, R. V. and Mitchell, R. W. 1982. Facies of the great American bank in the central Appalachians. Central Appalachian Geology, NE-SE GSA 1982 Fieldtrip #7.

Desrochers, A. 1983. Géologie du sectuer Ouest de l'archipel de Mingan. Ministre de l'Énergie et des Ressources, Québec, rapport préliminaire carte annotée, DP 83-04

Desrochers, A. 1984. Géologie du secteur Est de l'archipel de Mingan. Ministre de l'Énergie et des Ressources, Québec, rapport préliminaire carte annotée, DP 83-23.

Desrochers, A. 1985. The Lower and Middle Ordovician platform carbonates of the Mingan Islands, Quebec: stratigraphy, sedimentology, paleokarst and limestone diagenesis. Unpublished Ph. D. thesis, Memorial University of Newfoundland, St-John's, 454 p.

Desrochers, A. 1988. Stratigraphie de l'Ordovicien de la région de l'archipel de Mingan, Ministère de Québec, Direction générale de l'exploration géologique et minérale, MM 87-01.

Dickson, J. A. 1966. Carbonate identification and genesis as revealed by staining. Journal of Sedimentary Petrology, 36, 491-505.

Dix, G. R., Robinson, G. W., and McGregor, D. C. 1998. Paleokarst in the Lower Ordovician Beekmantown Group, Ottawa Embayment: structural control inboard of the Appalachian orogen. GSA Bulletin, 110, 1046-1059.

Dravis, J. J. 1990. Carbonate petrography—update on new techniques and applications, Journal of Sedimentary Petrology, 65, 626-627.

Dykstra, J. C. F. and Longman, M. W. 1994. Gas Reservoir Potential of the Lower Ordovician Beekmantown Group, Quebec Lowlands, Canada. AAPG Bulletin, 79, 513-530.

Folk, R. L. 1993. SEM imaging of bacteria and nannobacteria in carbonate sediments and rocks. Journal of Sedimentary Petrology, 63, 990-999.

Fortin, D. 1987. Contact Beekmantown-Chazy dans les Basses-Terres du St-Laurent: evaluation des effets de la discordance (Ordovicien Inférieur), unpublished Masters Thesis, Universite Laval, 63p

Friedman, I. and O'Neil, J.R., 1977. Compilation of stable isotope fractionation factors of geochemical interest. In: Data of Geochemistry. U.S. Geol. Surv., Prof. Pap., 440-KK, 6th ed.

Friedman, G. M. 1994. Upper Cambrian-Lower Ordovician (Sauk) platform carbonates of the Northern Appalachian (Gondwana) passive margin. Carbonates and Evaporites, 9, 143-150.

Gao, G. 1990. Petrography, geochemistry, and diagenesis of the Arbuckle Group, Slick Hills, SW Oklahoma. Unpublished Ph.D. dissertation, University of Texas, Austin, 162p.

Gao, G. and Land, L. 1991. Eraly Ordovician Cool Creek dolomite, Middle Arbuckle Group, Slickj Hills, SW Oklahoma, U.S.A.: origin and modification. Journal of Sedimentary Petrology, 61, 161-173.

Ginsburg, R. N. 1974. Introduction to comparative sedimentology. AAPG Bulletin, 58, 781-786.

Gournay, J. P.,Kirkland, B. l., Folk, R. L. and Lynch, F. L. 1999. Nanometer-scale features in dolomite from Pennsylvanian rocks, Paradox Basin, Utah, Sedimentary Geology, 126, 243-252.

Gregg, J. M. and Sibley, D. F. 1984. Epigenetic Dolomitization and the origin of xenotopic dolomite texture. Journal of Sedimentary Petrology, 54, 908-931.

Gregg J.M., Shelton, K. L., Johnson, A. J., Sommerville, I. D. and Wright, W. R. 2001. Dolomitization of the Waulsortian Limestone (Lower Carboniferous) in the Irish Midlands. Sedimentology, 48, 745-766.

Hardie, L. A. 1987. Dolomitization: a critical review of some current views. Journal of Sedimentary Petrology, 57, 166-183.

Harris, L. D. 1973. Journal of Research, US Geological Survey 1, 64p.

Haywick, D. W. 1984. Dolomite within the St. George Group, western Newfoundland, MSc Thesis, Memorial University. Stratigraphy.

Haywick, D. W. And James, N. P. 1984. Dolomite and dolomitization of the St. George Group, n, Current Research Part A, GSC Paper 84-1A, p. 531-536.

Holtz, M. H. and Kerans, C. 1992. Characterization and categorization of West Texas Ellenburger reservoirs. In Candelaria, M. P. and C. L. Reed, eds, Paleokarts and karst-related diagenesis and reservoir development; examples from Ordovician-Devonian age strata of West Texas and the mid-continent. SEPM 1992 field trip guidebook, Publication 92-33.

James, N. P., and Stevens, R. K. 1982. Anatomy and evolution of a Lower Paleozoic continental margin western Newfoundland. 11th International Congress on Sedimentology, Hamilton, Canada: Excursion 2B, 75p.

James, N. P., Barnes, C. R. and Stevens, R. K. 1989. A Lower Paleozoic continental margin carbonate platform, northern Canadian Appalachians, in Crevello, P. D., Wilson, J. L., Sarg, J.F. and Read, J. F., eds., Controls on carbonate platform and basin development, SEPM Special Publication, 44, 123-146.

James. N. P., Knight, I., Stevens, R. K. and Barnes, C. R. 1988. Sedimentology and Paleontology of an Early Paleozoic Continental Margin, Western Newfoundland. GAC-MAC, CSPG Field Trip Guide Book, Trip B1.

Kerans, C. 1989. Karst-controlled reservoir heterogeneity and an example from the Ellenburger Group (Lower Ordovician) of West Texas. Bureau of Economic Geology, The University of Texas at Austin, Report of Investigations No. 186. pp. 1-10.

Kesler, S. E. 1996. Appalachian Mississippi Valley-Type deposits: paleoaquifers and brine provinces, *in*, Sangster, Ed., Carbonate-Hosted Lead-Zinc Deposits. SEPM Special Publication No. 4, pp. 29-57.

Knight, I. and James, N. P. 1987. Stratigraphy of the St. George Group (Lower Ordovician), western Newfoundland: the interaction between eustacy and tectonics. Can J Earth Sciences, 24, 1927-1952.

Knight, I and James, N. P. 1988. Stratigraphy of the Lower to lower Middle Ordovician St. George Group, western Newfoundland. Newfoundland Department of Mines Report, 88-4, 48p.

Knight, I., James, N. P. and Lane, T. E. 1991. The Ordovician St. George unconformity, northern Appalachians: the relationship of plate convergence at the St. Lawrence Promontory to the Sauk-Tippecanoe sequence boundary: Geological Society of America Bulletin. 103, 1200-1225.

Kolkas, M. K. and Friedman, G. M. 1998. Diagenetic history and geochemistry of the Beekmantown-Group dolomites (Sauk Sequence) of New York, USA. Carbonates and Evaporites, 13, 69-85.

Kupecz, J.A. and Land, L.S. 1991. Late-stage dolomitization of the Lower Ordovician Ellenberger Group, west Texas. Journal of Sedimentary Petrology, 61, 551-574.

Kupecz, J. A., I. P. Montañez, and G. Gao, 1993. Recrystallization of dolomite with time In, R. Rezak and D. L. LaVoie, eds., Carbonate Microfacies: Springer-Verlag, New York, 187-194.

Kupecz, J.A. and Land, L.S. 1994. Progressive recrystallization and stabilization of early-stage dolomite: Lower Ordovician Ellenberger Groups, west Texas, In, Purser, B., ed. Dolomites: a Volume in Honour of Dolomieu, Special Publications, International Association of Sedimentologists, 21, 255-279.

Lane, T. E. 1990. Dolomitization, brecciation and zinc mineralogy and their paragenetic, stratigraphic and structural relationships in the Upper St. George Group (Ordovician) at Daniel's Harbour, Western Newfoundland. Unpublished Doctoral Thesis, Memorial University.

Lavoie, D. 1994. Diachronous tectonic collapse of the Ordovician continental margin, eastern Canada: comparison between the Quebec Reentrant and the St. Lawrence Promontory. Canadian Journal of Earth Sciences, 31, 1309-1319.

Lindsay, R. F. and Koskelin, K. M. 1991. Arbuckle Group depositional parasequences, southern Oklahoma. Oklahoma Geological circular, 92, 71-84.

Lohmann, K.C. and Walker, J.C.G. 1989. The $\delta^{18}O$ record of Phanerozoic abiotic marine calcite cements: Geophysical Research Letters, 16, 319-322.

Lumsden, D. N. and Caudle, C.G. 2001. Origin of massive dolostone: the Upper Knox model, Journal of Sedimentary Research, 71, 400-409.

Lynch, G. and Trollope, S. 2001. Dolomitization, platform collapse, and reservoir development in Ordovician carbonates of Anticosti Island, Gulf of St. Lawrence. Poster presentation to the C.S.P.G. annual technical convention "Rock the Foundation", June 18-21, program with abstracts pp. 126-1-126-6.

McKenzie, J. A. 1981. Holocene dolomitization of calcium carbonate sediments from the coastal sabkhas of Abu Dhabi, U.A.E.: a stable isotope study. Journal of Geology, 89, 185-198.

McCrea, J.M., 1950. On the isotope chemistry of carbonates and a paleotemperature scale, Jour. Chem. Physics, 18, 849-857.

Middleton, K., Coniglio, M., Sherlock, R. and Frape, S. K. 1993. Dolomitization of Middle Ordovician carbonate reservoirs, southwestern Ontario. Bulletin of Canadian Petroleum Geology, 41, 150-163.

Montañez I. P. 1992. Fluid-rock interaction history during stabilization of early dolomites, Upper Knox Group (Lower Ordovician), US Appalachians. Journal of Sedimentary Petrology, 62, 753-778.

Montañez, I. P. 1994. Late diagenetic dolomitization of Lower Ordovician, Upper Knox carbonates: a record of the hydrodynamic evolution of the southern Appalachian Basin. AAPG Bulletin, 78, 1210-1239.

Montañez, I. P. 1997. Application of cathodoluminescent cement stratigraphy for delineating regional diagenetic and fluid migration events associated with Mississippi valley-type mineralization in the southern Appalachians. In: D. F. Sangster, ed., Carbonate-hosted lead-zinc deposits. SEPM Special Publication 4, 432-447.

Montañez, I. P. and Read, J. F. 1992. Eustatic control on early dolomitization of cyclic peritidal carbonates: evidence from the Early Ordovician Upper Knox Group, Appalachians. Geological Society of America Bulletin, 104, 872-886.

Morin, C. 2001. Anticosti, Estuary and Gulf of St. Lawrence, Quebec, a petroleum region to be discovered! Oral presentation to the GAC/MAC Joint Annual Meeting, St. John's 2001, May 27-30, program with abstracts.

Nowlan, G. S. 1981. Stratigraphy and conodont faunas of the Lower and Middle Ordovician Romaine and Mingan Formations, Mingan Islands, Quebec. Maritime Sediments and Atlantic Geology; Abstract volume 17, p. 67.

Pratt, B. R. and James, N. P. 1986. The St. George Group (Lower Ordovician) of western Newfoundland: tidal flat island model for carbonate sediments in shallow epeiric seas. Sedimentology, 33, 313-344.

Radke, B. M. and Mathis, R. L. 1980. On the formation and occurrence of saddle dolomite. Journal of Sedimentary Petrology, 50, 1149-1168.

Read, J.F. 1989. Controls on evolution of Cambrian-Ordovician passive margins, U.S. Appalachians, in Crevello, P. D., Wilson, J. L., Sarg, J.F. and Read, J. F., eds., Controls on carbonate platform and basin development. SEPM Special Publication 44, 147-166.

Reimer, J.D. and Teare, M.R. 1992. Deep Burial Diagenesis and Porosity Modification in Carbonate Rocks by Thermalorganic Sulphate Reduction and Hydrothermal Dolomitization: TSR-HTD.; in 'Subsurface dissolution porosity in carbonates – recognition, causes and implications." C.S.P.G. short course #1, 1992 joint CSPG-AAPG convention, "Environments of Exploration", Calgary, Alberta., 41p.

Roksandic, M. M., and Granger, B. 1981. Structural styles of Anticosti Island, Gaspé Passage, and eastern Gaspé Penninsula inferred from reflection seismic data. In Subcommission on Silurian Stratigraphy, Ordovician-Silurian Boundary Working Group. Field meeting, Anticosti-Gaspé, 1981. Vol. II. Stratigraphy and paleontology. Ed. P. J. Lespérance. Université de Montréal, 211-221.

Rosenbaum, J., and Sheppard, S.M., 1986. An isotopic study of siderites, dolomites and ankerites at high temperatures. Geochim. Cosmochim. Acta, 50, 1147-1150.

Savard, M., Beauchamp, B. and Veizer, J. 1996. Significance of aragonite cements around Cretaceous marine methane seeps. Journal of Sedimentary Petrology, 66, 430-438.

Shaw, F. C. 1980. Shallow water lithofacies and trilobite lithofacies of the Mingan Formation (Ordovician), eastern Quebec. Le Naturaliste Canadien, 107, 227-242.

Schultze-Lam, S., Harauz, G., Beveridge, T. J. 1992. Participation of a cyanobacteria S layer in fine-grain mineral formation, Journal of Bacteriology, 174, 7971-7981.

Sibley, Duncan F. and Gregg, J. M. 1987. Classification of Dolomite Rock Textures. Journal of Sedimentary Petrology, 57, 967-975.

SOQUIP. 1983. Rapport technique statutaire île d'Anticosti. Centre de la diffusion de la géoinformation, Ministére de l'Énergie et des Ressources du Québec, rapport SOQUIP no 13129.

Stenzel, S. R., Knight, I., and James, N. P. 1990. Carbonate platform to foreland basin: revised stratigraphy for the Table Head Group (Middle Ordovician), western Newfoundland. Canadian Journal of Earth Science, 27, 14-26.

Thomas, W. A. 1977. Evolution of Appalachian-Ouachita salients and recesses from reentrants and promontories in the continental margin. American Journal of Science, 277, 1233-1278.

Thompson, J. B. and Ferris, F. G. 1990. Cyanobacterial precipitation of gypsum, calcite, and magnesite from natural alkaline lake water, Geology, 18, 995-998.

Tucker, M. E. and Wright, V. P. 1990. Carbonate Sedimentology. Blackwell Scientific Publications, Boston. 484p.

Twenhofel, W. H. 1938. Geology and Paleontology of the Mingan Islands, Quebec. GSA Bulletin, 42, 575-588.

Vasconcelos, C., McKenzie, J. A., Bernasconi, S., Grujic, D. and Tien, A. J.. 1995. Microbial mediation as a possible mechanism for natural dolomite formation at low temperatures, Nature, 377, 220-222.

Vasconcelos and McKenzie, J.A. 1997. Microbial mediation of modern dolomite, precipitation and diagenesis under anoxic conditions (Lagoa Vermelha, Rio de Janeiro, Brazil), Journal of Sedimentary Research, 67, 278-290.

Veizer, J., D. Ala, K. Azmy, P. Bruckschen, D. Buhl, F. Bruhn, G. A. F. Carden, A. Diener, S. Ebneth, Y. Godderis, T. Jasper, C. Korte, F. Pawellek, O. G. Podlaha and H. Strauss. 1999. $^{87}Sr/^{86}Sr$, $\delta^{13}C$ and $\delta^{18}O$ evolution of Phanerozoic seawater, Chemical Geology, 161, 59-88.

Walker, R. G. and N. P. James, (Eds.). 1992. Facies Models: response to sea level change. Geological Association of Canada, 454p.

Wanless, H. R. 1979. Limestone response to stress: pressure solution and dolomitization. Journal of Sedimentary Petrology, 49, 437-462.

Warren, J. 2000. Dolomite: occurrence, evolution and economically important associations, Earth Science Reviews, 52, 1-81.

Williams, H., Dehler, S. A., Grant, A. C., and Oakey, G. N. 1999. Tectonics of Atlantic Canada. Geoscience Canada, 26, 51-70.

Wright, D. T. 1999. The role of sulphate reducing bacteria and cyanobacteria in dolomite formation in distal ephemeral lakes of the Coorong regions, South Australia, Sedimentary Geology, 126, 147-157.